

1.65 μm (H-band) surface photometry of galaxies. VIII: the near-IR κ -space at $z=0$

D. Pierini¹, G. Gavazzi², P. Franzetti², M. Scodeggio³ and A. Boselli⁴

¹*Dept. of Physics and Astronomy, The University of Toledo, 2801 W. Bancroft, 43606, Toledo, Ohio*

²*Università degli Studi di Milano - Bicocca, P.zza dell'Ateneo Nuovo 1, I-20126, Milano, Italy*

³*IFCTR/CNR, Via Bassini 15, I-20133, Milano, Italy*

⁴*Laboratoire d'Astrophysique de Marseille, BP8 Traverse du Syphon, F-13376, Marseille, France*

Accepted ... Received ...; in original ...

ABSTRACT

We present the distribution of a statistical sample of nearby galaxies in the κ -space ($\kappa_1 \propto \log M$, $\kappa_2 \propto \log I_e$, $\kappa_3 \propto \log M/L$). Our study is based on near-IR (H-band: $\lambda = 1.65 \mu\text{m}$) observations, for the first time comprising early- and late-type systems. Our data confirm that the mean effective dynamical mass-to-light ratio M/L of the E+S0+S0a galaxies increases with increasing effective dynamical mass M , as expected from the existence of the Fundamental Plane relation. Conversely, spiral and Im/BCD galaxies show a broad distribution in M/L with no detected trend of M/L with M , the former galaxies having M/L values about twice larger than the latter, on average. For all the late-type galaxies, the M/L increases with decreasing effective surface intensity I_e , consistent with the existence of the Tully–Fisher relation. These results are discussed on the basis of the assumptions behind the construction of the κ -space and their limitations. Our study is complementary to a previous investigation in the optical (B-band: $\lambda = 0.44 \mu\text{m}$) and allows us to study wavelength-dependences of the galaxy distribution in the κ -space. As a first result, we find that the galaxy distribution in the κ_1 – κ_2 plane reproduces the transition from bulge-less to bulge-dominated systems in galaxies of increasing dynamical mass. Conversely, it appears that the M/L of late-types is higher (lower) than that of early-types with the same M in the near-IR (optical). The origins of this behaviour are discussed in terms of dust attenuation and star formation history.

Key words: galaxies: spiral – galaxies: elliptical and lenticular – galaxies: fundamental parameters – galaxies: stellar content – infrared: galaxies.

1 INTRODUCTION

The study of the scaling relations between photometric and kinematical properties of present-day stellar systems is a powerful tool for the comprehension of the processes that led to their formation and evolution (e.g. Mao & Mo 1998; Mao, Mo & White 1998; Pahre, de Carvalho & Djorgovski 1998; Avila-Reese & Firmani 2000). The relation between the total luminosity L and the central velocity dispersion σ_0 (Faber & Jackson 1976) and the relation between the effective radius r_e (the radius that contains half of the galaxy total luminosity) and the central surface brightness μ_0 (Kormendy 1977) represent benchmarks for any theoretical modelling of the early-type galaxies (de Zeeuw & Franx 1991 and references therein). Further analyses pointed out that these galaxies and the bulges of the spiral galaxies populate a two-dimensional manifold in the parameter space defined by r_e , μ_e and σ_0 , named the Fundamental Plane (FP)

(Djorgovski & Davis 1987; Dressler et al. 1987), where μ_e is the mean effective surface brightness (mean surface brightness within r_e). The profound implications of this result, its interpretation and its extension to parent systems at high redshifts are still grounds both of observational challenge and of intellectually exciting debate (e.g., Scodeggio et al. 1998; Pahre, Djorgovski & de Carvalho 1999 and references therein). For the late-type galaxies, the correlation between the total luminosity L and the maximum rotational velocity V_{Max} (Tully & Fisher 1977), as well as the distribution in the parameter space defined by exponential disk scale-length h and central surface brightness μ_0 (Grosbøl 1985; de Jong 1996a; see also Pierini 1997) are now compelling for any theory of disk-galaxy formation (e.g. Dalcanton, Spergel & Summers 1997; Mo, Mao & White 1998; Syer, Mao & Mo 1999). In order to reproduce the locus of these systems in the h – μ_0 plane, a bivariate distribution in mass and spin parameter of the proto-galaxies is required, whatever the

model of disk-galaxy formation is (cf. Dalcanton, Spergel & Summers 1997; Firmani & Avila-Reese 2000).

The effective and central photometric parameters involved by the previous scaling relations were determined traditionally from fitting either a de Vaucouleurs $r^{1/4}$ law (de Vaucouleurs 1948) or an exponential law (Freeman 1970) to the radial surface brightness profiles. The first law was used to describe the light distribution along the radial coordinate of the elliptical galaxies and of the bulges of the spiral galaxies, after the pioneering analyses of de Vaucouleurs (1948, 1959). The second one was found to be a good description of the light profiles of the disks, also in the case of S0 galaxies (Burstein 1979).

Burstein et al. (1997 – hereafter referred to as BBFN; see also Bender, Burstein & Faber 1992; Burstein et al. 1995) proposed a three-dimensional parameter system, called κ -space, in order to represent and to compare the global relationships of any stellar system (i.e., from the Galactic globular clusters to the galaxy clusters), in a self-consistent way. The axes of the κ -space, κ_1 , κ_2 and κ_3 , are proportional to the logarithms of the galaxy mass and mass-to-light ratio and of a third quantity, which is basically the surface brightness, respectively, and do not depend on the fitting law of the surface brightness profile. They reflect a set of physical assumptions on the structure and velocity pattern of the different self-gravitating, equilibrium stellar systems (see BBFN), which may be subject of criticism on the basis of some observational results (e.g. Caon, Capaccioli & D’Onofrio 1993; Busarello et al. 1997). BBFN investigated kinematical and structural properties of nearby galaxies on the basis of a large optical (B-band: $\lambda = 0.44 \mu\text{m}$) dataset. Further analyses focussed on the distribution in the near-IR κ -space either of present-day E+S0 systems (Pahre, Djorgovski & de Carvalho 1998 – hereafter referred to as PDdC) or of disks and bulges of present-day late-type galaxies (Moriondo, Giovanelli & Haynes 1999). The adoption of near-IR photometry gives an insight of the scaling properties of galaxies less biased by differences in age and metallicity of the stellar populations (de Jong 1996b) and by dustiness (Cardelli, Clayton & Mathis 1989 and references therein) than the picture emerging from optical studies.

Here we present the near-IR (H-band: $\lambda = 1.65 \mu\text{m}$) κ -space of both early- and late-type galaxies as a whole at $z=0$. In Sect. 2 we define the κ -space axes and their relations with typical galaxy parameters, such as mass, radius, surface brightness and luminosity, and discuss the physical assumptions behind the κ -space and their limitations. The selection criteria of our sample and the determination of the galaxy parameters involved by the definition of the κ -space axes are described in Sect. 3. Here we note that this sample comprises several Virgo cluster galaxies down to $M_B = -15 \text{ mag}$ (cf. Boselli et al. 1997, 2000a), though it is not complete to low surface brightness and dwarf galaxies. We present and discuss the galaxy distribution in the near-IR κ -space in Sect. 4. Discussion and conclusions on the wavelength-dependence of the galaxy distribution in the κ -space are given in Sect. 5.

2 PHYSICAL MEANING OF THE κ -SPACE PARAMETERS: ASSUMPTIONS AND THEIR LIMITATIONS

In origin (Bender, Burstein & Faber 1992), the κ -space is a representation of the structural properties of the elliptical galaxies (but also of bulges of S0 and spiral galaxies) which makes use of a particular orthogonal rotation of the global parameter space defined by the one-dimensional central velocity dispersion (σ_0), effective radius (r_e) and mean effective surface intensity (I_e). This orthogonal rotation provides face-on and edge-on views of the Fundamental Plane, under the assumption that the ellipticals form a homologous family, i.e., that the two structure parameters c_1 and c_2 , which define the total luminosity L_T ($L_T = c_1 I_e r_e^2$) and the total mass M_T ($M_T = c_2 \sigma_0^2 r_e$) of the system, are constant. As a consequence, it implies the following logarithmic relations between the three κ -coordinates κ_1 , κ_2 and κ_3 and the parameters σ_0 , r_e and I_e of the early-type galaxies:

$$\kappa_1 = (\log \sigma_0^2 + \log r_e) / \sqrt{2} \quad (1)$$

$$\kappa_2 = (\log \sigma_0^2 + 2 \log I_e - \log r_e) / \sqrt{6} \quad (2)$$

$$\kappa_3 = (\log \sigma_0^2 - \log I_e - \log r_e) / \sqrt{3}, \quad (3)$$

where r_e is in kpc, I_e is in solar units and σ_0 is in km s^{-1} .

While $c_1 = 2\pi$, by definition of I_e , the assumption of a constant c_2 is more uncertain and, therefore, plays a more fundamental role. Bender, Burstein & Faber calculated that c_2/c_1 decreases by about a factor 1.6 from dwarf ellipticals to giant ellipticals in a roughly monotonic fashion, under the assumption that ellipticals are described by King (1966) models with an isotropic velocity dispersion. Of course real ellipticals may have more complex internal kinematics. The debate on homology is still waiting for definitive answers, but from theoretical (Capelato, de Carvalho & Carlberg 1995, 1997) and observational (Graham & Colless 1997; Busarello et al. 1997) studies it seems to emerge that kinematical deviations from a homologous family may produce more important effects than structural deviations (see also Pahre, de Carvalho & Djorgovski 1998).

Successively, BBFN proposed the κ -space as a tool of representation of the structural properties of all stellar systems. In particular, for spiral and irregular galaxies, this required the adoption of a transformation from their characteristic velocity at r_e to their central velocity dispersion σ_0 , their r_e and I_e being defined as for the ellipticals. Under the assumption that spiral and irregular galaxies have exponential Freeman (1970) disks and central surface brightnesses within 1 mag arcsec $^{-2}$ of 21.65 B-mag arcsec $^{-2}$, the characteristic velocity at r_e is reasonably assumed to be equal to the maximum rotational velocity V_{Max} , on the basis of the observational results of Rubin et al. (1985). The transformation from V_{Max} to σ_0 adopted by BBFN (i.e., $V_{Max}/\sigma_0 = \sqrt{2}$) descends from the further assumption that disks are embedded in isotropic isothermal halos (Binney & Tremaine 1987, Equ. 4-55), and is consistent with observed values of this ratio (Whitmore & Kirshner 1981). With this transformation, the κ -coordinates of spiral and irregular galaxies are given by:

$$\kappa_1 = (\log V_{Max}^2 + \log r_e) / \sqrt{2} - 0.21 \quad (4)$$

$$\kappa_2 = (\log V_{Max}^2 + 2 \log I_e - \log r_e) / \sqrt{6} - 0.12 \quad (5)$$

$$\kappa_3 = (\log V_{\text{Max}}^2 - \log I_e - \log r_e) / \sqrt{3} - 0.17, \quad (6)$$

where V_{Max} is expressed in km s^{-1} .

According to the previous assumptions, the dynamical mass and the dynamical mass-to-light ratio of any early- and late-type galaxy within r_e may be expressed in terms of the definitions 1–6 of the κ -coordinates. The effective dynamical mass (i.e., the mass within r_e) is defined by $M_e = 4.65 \times 10^5 \sigma_0^2 r_e M_\odot$, where the standard Keplerian formula $M_e = r_e V^2(r_e)/G$ is adopted in order to define the mass of a disk, with $V(r_e)$ set equal to V_{Max} and transformed to σ_0 . As a consequence, the effective dynamical mass (in solar units) is given by:

$$\log M_e(M_\odot) = \sqrt{2}\kappa_1 + 5.67. \quad (7)$$

From the definition of effective luminosity (i.e., the luminosity within r_e) $L_e = \pi \times 10^6 I_e r_e^2$,

$$\log L_e(L_\odot) = \sqrt{2}\kappa_1 - \sqrt{3}\kappa_3 + 6.50, \quad (8)$$

so that the effective dynamical mass-to-light ratio is expressed as:

$$\log M_e/L_e (\odot) = \sqrt{3}\kappa_3 - 0.83. \quad (9)$$

In elliptical (and lenticular) galaxies, neglect of rotational support and flattening may lead to the underestimation of M , as derived from Equ. 7. The fractional contribution of ordered motion (rotation) to the total kinetic energy is not negligible in elliptical galaxies of intermediate mass (BBFN). In recent years (Simien & Prugniel 2000 and references therein), it has been found that, in elliptical galaxies, the ratio of rotational velocity and velocity dispersion has a broad range, with an average value of the order of 40%, roughly. For an isotropic oblate rotator, this figure corresponds to a fractional change in kinetic energy due to rotation of about 5%, which is associated with an ellipticity less than 0.2 (Binney & Tremaine 1987). According to the computational results tabulated by the latter authors, the correction factor for the mass of a rotating oblate galaxy with the previous characteristic is less than 1.12, i.e., 0.05 dex. As a reference, for rotating ellipticals of maximum ellipticity ~ 0.4 , the theoretical mass correction is 1.35, i.e., 0.13 dex.

The assumptions made in the case of spiral and irregular galaxies affect the κ -coordinates of these stellar systems as well. One reason of concern is that these objects are far from being described by a Freeman exponential profile in a homogeneous way, and not only when a bulge is present. In fact, in the near-IR, the central surface brightness of the disk-component of spiral and irregular galaxies falls within a broad range of $\sim 4 \text{ mag arcsec}^{-2}$ (Grosbøl 1985; de Jong 1996a; Pierini 1997). Moreover, the effective radius of a spiral galaxy depends on the bulge-to-disk ratio in a complex way, this ratio depending on the formation mechanisms of bulge and disk, and on the spectral energy distribution of each of these two components. On a statistical basis, Gavazzi et al. (2000b – hereafter referred to as Paper V) and Scodreggio et al. (2001 – hereafter referred to as Paper IX) have found that the central near-IR-light concentration increases with near-IR luminosity in spiral and irregular galaxies. Consistently, more luminous systems tend to have a bulge. This means that, for these stellar systems, the effective radius corresponds to a lower fraction of

the isophotal radius with increasing luminosity. The radius where the (supposed) universal shape of the rotation curve of spiral galaxies reaches its maximum velocity changes with luminosity as well (Persic, Salucci & Stel 1996), this radius becoming much shorter than the isophotal optical radius with increasing luminosity. On one hand, these results support the assumption that $V(r_e) = V_{\text{Max}}$ in spiral galaxies with a bulge. Therefore, Equ. 7 and 8 may be applied to spiral galaxies with a bulge, the more luminous ones, on average, the principal unknown being whether the transformation from V_{Max} to σ_0 changes for these systems, i.e., more generally, with luminosity. On the other hand, the same assumption may be made for spiral and irregular galaxies of lower luminosities since the rotation pattern of these objects becomes shallow at radii $\geq r_e$ (Persic, Salucci & Stel 1996), with the caveat that, by imposing $V(r_e) = V_{\text{Max}}$, $V(r_e)$ may be significantly overestimated in the least luminous objects.

3 DATA

3.1 Sample and data analysis

In the last 7 years, Gavazzi and collaborators have carried out an extensive imaging survey of 1157 early- and late-type galaxies of the Local Universe, in the near-IR bands H and/or K' ($\lambda = 2.10 \mu\text{m}$). The sample galaxies were optically selected in regions of the A262, Cancer and Virgo clusters, and of the Coma Supercluster (cf. Gavazzi, Pierini & Boselli 1996 – hereafter referred to as GPB). We determine galaxy distances either from individual redshifts using $H_0 = 75 \text{ km s}^{-1} \text{Mpc}^{-1}$ (isolated galaxies of the Coma Supercluster and Cancer cluster members) or via the cluster assignment method, i.e. from the average redshift of the structure to which they belong (cf. GPB). According to the different estimated distances and adopted limiting magnitudes, only for the Virgo cluster subsample (Boselli et al. 1997, 2000a) the observations reach the bright end of the luminosity function of dwarf systems. We identify dwarf systems as those which satisfy the commonly accepted distance-luminosity definition of Tammann (1980).

The entire survey is described in details elsewhere (Gavazzi et al. 1996b,c; Boselli et al. 1997; Scodreggio et al. 1998; Gavazzi et al. 2000a; Boselli et al. 2000a – hereafter referred to as Papers I and II, B97, S98, Papers III and IV) and we refer the reader to these papers for details concerning observations, data reduction, photometric calibration and image reduction procedures of these 1157 galaxies. For the present study it is important to say that azimuthally averaged surface brightness profiles were derived and successively fitted using either a de Vaucouleurs $r^{1/4}$ law, an exponential-law, a bulge+disk model or an exponential/de Vaucouleurs truncated model. The total magnitude of each galaxy was obtained by adding to the flux measured within the outermost significant isophote the flux extrapolated to infinity along the model that fitted the outer parts of the galaxy. The typical internal error in the determination of H_T is $\pm 0.15 \text{ mag}$. The effective radius r_e and the mean surface brightness within r_e (i.e., μ_e) of each galaxy were computed in two ways (Paper V). The “fitted” values of the individual components were derived from the individual fitted profiles, extrapolated to zero and to infinity. By contrast, the “empirical” values of the effective radius and surface brightness

of the system were obtained locating the half-light point along the observed light profile, where the total amount of light is given by the total magnitude described above, and corrected for seeing according to Saglia, Bender & Dressler (1993). The “empirical” values of r_e and μ_e are used here. Typical internal errors in the determination of $\log r_e$ and μ_e are ± 0.05 and ± 0.16 mag arcsec $^{-1}$, respectively. Empirical values of the radii that enclose 75% and 25% of the total light were also determined, and their ratio defines the concentration index c_{31} (de Vaucouleurs 1977). Since part of the late-type galaxies in the Virgo cluster were observed in the K'-band, their surface brightness profiles were corrected for the mean H-K' color term found by B97 (0.26 mag) before the determination of r_e and μ_e .

For the late-type galaxies, accurately determined (double or single horned profile with high signal-to-noise ratio) line-widths (a mean of the full-widths at the 20% and 50% levels of the maximum intensity) are taken from homogeneous low spatial resolution HI (i.e., $\lambda = 21$ cm) spectroscopic data-sets available in the literature (Scodreggio & Gavazzi 1993 and references therein). In absence of 21 cm measurements or for HI-deficient spirals (Haynes & Giovanelli 1984), maximum rotational velocities are derived from optical (i.e., H α line, $\lambda = 6563$ Å) major-axis rotation curves either derived by us (Gavazzi et al. 1999) or available in the literature. Reassuringly, no evidences of systematic differences in the measured line-widths either from HI or from H α spectroscopic data are found for the subsample of non HI-deficient objects with both measurements (Gavazzi et al. 1999). The values of V_{Max} are derived from the line-widths, corrected for turbulent/z-motions along the line-of-sight (-12.6 km s $^{-1}$) according to Richter & Huchtmeier (1984) and deprojected according to the Hubble type-dependent Holmberg formula given by Haynes & Giovanelli (1984). For the early-type galaxies, the values of the velocity dispersion are taken from the literature (S98 and references therein) and homogenized, if necessary, according to the latter authors.

In the present analysis, we exclude the dE and dS0 galaxies observed by Gavazzi et al. (2001) since it is still matter of debate whether their stellar disk-component is rotationally flattened or not (e.g. Rix, Carollo & Freeman 1999; Geha, Guhathakurta & van der Marel 2001). By contrast, we select 197 early-type galaxies and 210 late-type galaxies, out of the surveyed sample of 1157 galaxies, according to the following criteria:

- 1) available homogeneous reliable measurements either of the central velocity dispersion or of the maximum rotational velocity, for early- and late-type galaxies, respectively;
- 2) (only for the late-type systems) galaxy inclination between 30° and 85° , in order to limit any deprojection bias on V_{Max} and a non-negligible inclination correction of the photometric properties (if any), respectively;
- 3) goodness of the mono-dimensional (i.e. radial) surface brightness profile fit (Paper V), assured by the rejection threshold $\chi^2 = 3.5$. Though r_e and μ_e do not come from the fitting of the radial surface brightness profile, we adopt this criterion in order to select a sample of “well-behaved” galaxies, i.e. of objects with photometric properties not highly affected either by prominent structural features different from bulge and disk or by peculiarities.

Requirement 1 limits the statistics of our sample by

and large, so that we do not adopt any cut either in V_{Max} or in σ_0 , though literature sources suggest that values of $V_{Max} < 100$ km s $^{-1}$ and of $\sigma_0 < 100$ km s $^{-1}$ are less reliable (but see PDdC). The availability of reliable measurements of V_{Max} limits the statistics of galaxies later than Sc but not that of S0a–Sab galaxies.

No completeness is claimed for the resultant sample of 407 galaxies, which is, therefore, exposed to the cluster population incompleteness bias (Teerikorpi 1987, 1990). Since the goal of the present paper is not to determine statistically accurate relations between the parameters of different scaling relations but to discuss the relative distribution of each morphological class of galaxies within the κ -space, the effects of such a bias are less worrisome.

For the sample here selected, Table 1 reproduces the relevant information as follows:

- 1) the galaxy denomination, from either the “Catalogue of Galaxies and Clusters of Galaxies” of Zwicky et al. (1961–1968 – CGCG) or from the “Virgo Cluster Catalogue” of Binggeli, Sandage & Tammann (1985 – VCC);
- 2) the Hubble type (0 = E – E/S0, 1 = S0, 2 = S0a – S0/Sa, 3 = Sa, 4 = Sab, 5 = Sb, 6 = Sbc, 7 = Sc (dSc), 8 = Scd, 9 = Sd, 10 = Sdm – Sd/Sm, 11 = Sm, 12 = Im (Im/S), 13 = generic irregulars of Coma and peculiar galaxies, 14 = S/BCD (dS/BCD, dS0/BCD, Sd/BCD), 15 = Sm/BCD, 16 = Im/BCD);
- 3) the major axis;
- 4) the minor axis;
- 5) the characteristic velocity (i.e., either the central velocity dispersion σ_0 or the maximum rotational velocity V_{Max} according to morphology);
- 6) the effective radius r_e ;
- 7) the effective surface brightness μ_e (the effective surface intensity in H-band solar units is given by $I_e = 10^{-0.4(\mu_e - 24.91)}$);
- 8) κ_1 ;
- 9) κ_2 ;
- 10) κ_3 .

The values of r_e and μ_e listed in Tab. 1 are corrected for extinction as described in the next section.

3.2 Extinction corrections

Dust extinction affects the observed global metric and photometric properties of potentially any galaxy somehow, since dust production is a result of star formation. The magnitude of these effects changes with the pass-band of the observations and depends on the physical and chemical properties of the dust grains, the topology of the dust, the distribution of the dust with respect to the different stellar populations and the attenuation optical depth along the line-of-sight in a non trivial way. A careful correction of the photometric properties for dust attenuation, in particular, requires modeling of the stellar populations and of the radiative transfer within each galaxy, on one hand, and a multi-wavelength data-set for any individual galaxy, on the other. This task is prohibitive for a large sample like ours. Therefore, we have to make a set of assumptions and adopt a set of corrections based on statistics. The relatively low extinction in the H-band (Cardelli, Clayton & Mathis 1989 and references therein) gives some insurance against large systematic

errors, though the magnitude of the error may vary on an individual basis.

Elliptical and lenticular galaxies may contain dust, either in the form of lanes and patches or of a diffuse component of the interstellar medium (Bertola & Galletta 1978; Hawarden et al. 1981; Jura 1986). The wavelength-dependent effects of dust absorption and scattering on their photometric properties have been studied by Witt, Thronson & Capuano (1992) under the assumption of a diffuse dust component. As shown by these authors, attenuation optical depths of 0.1–1 in the V-band ($\lambda = 0.55 \mu\text{m}$) may explain some of the photometric properties of these stellar systems, e.g. their color gradients. Starlight attenuation is primarily the result of absorption in the near-IR, where the absorption optical depths are lower than in the optical (Witt, Thronson & Capuano). Dust is found capable to affect the projection of the kinematical quantities of these stellar systems as well (Baes & Dejonghe 2000; Baes, Dejonghe & De Rijcke 2000). Nonetheless, under the assumption that only the diffuse dust component is present in elliptical and lenticular systems, we may reasonably assume that these stellar systems are basically dust-free in the H-band, in agreement with Baes & Dejonghe.

This assumption is questionable for spiral and irregular galaxies. The debate on the opacity of the disk-component of spiral and irregular galaxies is still open and its discussion is beyond our scope (see Disney et al. 1989 for a review). If dust is distributed only in the disk, disks are more absorbed at high inclinations, because of the larger optical depth of the dust in the plane of the galaxy. By contrast, bulges are more attenuated at low inclinations, as in this case basically only the foreground light of the system is observed, whereas at high inclinations, almost the entire bulge comes into view, if the dust thickness is not substantial with respect to the bulge effective radius (Ferrara et al. 1999). As a consequence, in bulge+disk systems, the dust effects on r_e and μ_e will depend not only on the opacity along the line-of-sight but also on the bulge-to-disk ratio at a given pass-band. To make things more complex, bulges may be dusty too (Peletier et al. 1999). For bulge+disk systems, recipes for the correction of r_e and μ_e for dust attenuation, motivated either by radiative transfer models or by observational studies, still lack. By contrast, dust attenuation in exponential disks has driven more attention both from theory (e.g. Bianchi et al. 2000) and observations (e.g. Moriondo, Giovanelli & Haynes 1999). For the purposes of our study, we make the following assumptions: i) dust is distributed only in the disk-component of spiral and irregular galaxies; ii) the inclination corrections for r_e and μ_e are the same as for the exponential disk scale-length (h) and central surface brightness (μ_0), respectively, whatever the late Hubble type of the galaxy is. Given the previous discussion, we acknowledge that the second assumption over-simplifies the problem. However, at least this assumption does not lead to an inconsistency when we compare the effective luminosities obtained through Equ. 10, after applying the extinction correction of Moriondo, Giovanelli & Haynes (1999) to r_e and μ_e , and the total luminosities obtained from our data analysis and corrected for internal extinction (Galactic extinction is negligible in the H-band) according to the recipes of Gavazzi & Boselli (1996). The corrections for inclination applied to r_e and μ_e are:

$$r_{e,c} = r_{e,o} / (1 + 0.41(\pm 0.17) \log a/b) \quad (10)$$

$$\mu_{e,c} = \mu_{e,o} + 1.5(\pm 0.35) \log a/b, \quad (11)$$

where $r_{e,o}$, $r_{e,c}$, $\mu_{e,o}$ and $\mu_{e,c}$ are the observed and corrected values of the effective radius (in arcsec) and of the mean effective surface brightness (in mag arcsec⁻²), respectively, and a/b is the major-to-minor axis ratio. Total magnitudes are corrected for internal extinction as follows (Gavazzi & Boselli 1996):

$$m_{T,c} = m_{T,o} - 2.5 \times 0.17 \log a/b, \quad (12)$$

where $m_{T,o}$ and $m_{T,c}$ are the observed and corrected values, whatever the Hubble-type is. In fact, Gavazzi & Boselli did not find any morphological dependence of the corrections of total magnitudes for internal extinction in the near-IR pass-bands, as opposed to the optical ones.

4 THE H-BAND K-SPACE

Fig. 1 shows the distribution of the sample galaxies in a three-dimensional fold-out of the near-IR κ -space. Here we group the sample galaxies in ellipticals (E) plus lenticulars (S0), S0a galaxies, and giant spirals (Sa–Sc) plus late-spirals/Im/BCDs (Scd–Im/BCD) and generic irregular/peculiar galaxies. E+S0, S0a, Sa–Im/BCD galaxies plus generic irregular/peculiar galaxies are represented with filled circles, asterisks and empty circles, respectively, in Fig. 1. We assume characteristic cumulative uncertainties $\delta\kappa_1 = \delta\kappa_2 = \delta\kappa_3 = 0.1$, consistent with typical uncertainties in the observables (cf. Sect. 3). The magnitudes of these 1σ errors are reproduced in each panel of Fig. 1. We also reproduce the increase in all the three κ -space coordinates due to the increase of the dynamical mass when the potential contribution of rotational velocity to the total kinetic energy of the ellipticals is taken into account (cf. Sect. 2).

Here we need to say that the impact of the extinction corrections on the distribution of the late-type galaxies in the near-IR κ -space is small but the fact that the average effective mass-to-light ratio of these galaxies increases by 70% when extinction corrections are applied.

In the next subsections we analyse the galaxy distribution in each projection of the κ -space as a function of morphology. Therefore, in Fig. 2, we reproduce the three-dimensional fold-out of the near-IR κ -space for these four groups of Hubble types:

- E, S0 and S0a, represented by filled circles, empty squares and asterisks, respectively (panel a);
- Sa+Sab and Sb, represented by broad crosses and empty hexagons, respectively (panel b);
- Sbc and Sc, represented by filled triangles and empty circles, respectively (panel c);
- Scd, Sd and Im/BCD plus generic irregular/peculiar galaxies, represented by empty pentagons, stars and crosses, respectively (panel d).

We adopt this classification from BBFN (except for the generic irregular/peculiar galaxies).

In each panel of Fig. 2, we reproduce the Fundamental Plane relation in the κ_1 – κ_3 plane (see Sect. 4.1.1), the distribution of the E+S0 galaxies, within $\pm 1\sigma$ from the mean,

in the κ_2 – κ_3 plane (see Sect. 4.2.1) and the borderline of the “Zone of Exclusion” in the κ_1 – κ_2 plane (see Sect. 4.3.1).

4.1 Galaxies in the κ_1 – κ_3 plane

4.1.1 Ellipticals and lenticulars

The distribution of the elliptical and lenticular galaxies in the κ_1 – κ_3 projection of the κ -space confirms that the dynamical mass-to-near-IR light ratio increases with the dynamical mass (cf. PDdC) as found in the optical (Bender, Burstein & Faber 1992; Burstein et al. 1995; BBFN). This result was expected from the existence of the Fundamental Plane relation in its canonical notation (Pahre, de Carvalho & Djorgovski 1998; S98). A linear fit to the data which minimizes the dispersion in both axes gives:

$$\kappa_3 = 0.242(\pm 0.022)\kappa_1 - 0.373(\pm 0.076). \quad (13)$$

The slope of the H-band FP (in κ -space notation) that we derive corresponds to the scaling relations $M_e/L_e \propto M_e^{0.296 \pm 0.027}$ and $M_e/L_e \propto L_e^{0.421 \pm 0.055}$. In the K-band PDdC obtained $M_e/L_e \propto M_e^{0.147 \pm 0.011}$ and $M_e/L_e \propto L_e^{0.172 \pm 0.013}$. The origin of the significant discrepancy between these two sets of near-IR scaling relations is twofold: the incompleteness bias and differences in data analysis. First we note that both these analyses rest on incomplete samples, so that the derived scaling relations are biased. The PDdC sample is more than twice in size than ours, containing 251 elliptical and lenticular galaxies, selected primarily from 13 nearby rich clusters (but also from loose groups and the general field), whose distribution in redshift velocity brackets the redshift velocities of Virgo and Coma, the main contributors of objects in our study. According to the study of the incompleteness bias by Teerikorpi (1987, 1990), we may allow that, in our sample, the fraction of low-luminosity (and low-mass) objects is skew towards higher luminosities (and masses) than in the PDdC sample, so that a steeper relation between mass-to-light ratio and mass may be expected. Nonetheless, systematic differences in the data analysis between us and PDdC probably have a larger impact on the obtained scaling relations. While the seeing corrections adopted by us and PDdC are consistent (cf. Pahre 1999), the effective radii and mean surface brightnesses are derived in two different ways. We obtain these effective parameters from isophotal, elliptical surface photometry (cf. Sect. 3.1), while PDdC determined them from circular aperture photometry, in agreement with previous optical studies. As discussed by Pahre (1999), the isophotal estimate of the effective radius is, on average, slightly larger than its circular aperture estimate, and, conversely, the isophotal estimate of the effective intensity is lower than the corresponding circular aperture estimate. This was already proposed by S98 in order to explain the discrepancy between the H-band and the K-band FP relations, the K-band effective parameters being obtained from the circular aperture estimates of Mobasher et al. (1999). If the comparison of these two datasets is held as representative of the systematic effects due to the different data analysis, we infer that the adoption of circular aperture estimates of the effective parameters causes a systematic decrease of the κ_1 and κ_3 coordinates (cf. Equ. 1 and 3). This results in a reduced slope of the FP in the

κ -space notation and contributes to justify the discrepancy between us and PDdC.

4.1.2 Spirals and Im/BCDs

Spiral and Im/BCD galaxies form two distinct classes in the κ_1 – κ_3 plane, the latter having a mean effective mass-to-light ratio (in solar units) larger by a factor of 2. Taken as a whole, the late-type galaxies have a mean value of κ_3 equal to 0.656, i.e., a mean effective mass-to-light ratio (in solar units) equal to 2. This figure is 43% of the value of the mean total mass-to-light ratio (in solar units) determined by GPB for a sample of 426 late-type galaxies. This large discrepancy has not a statistical origin. First, the total mass-to-light ratios of GPB were determined, under the same assumptions of virial equilibrium and spherical symmetry as in Sect. 2, at the 25 B-mag arcsec^{−2} isophotal radius R_{opt} , and not at infinity. As a consequence, the mass-to-light ratios quoted in GPB are about 10% less than the total ones, on average. From the definitions of total and effective mass and luminosity, M_T and L_T respectively, it is straightforward to determine that $M_e/L_e = 2r_e/R_{opt} \times M_T/L_T$. Whatever the Hubble type of the galaxy is, on average, $R_{opt}/r_e = 5.3 \pm 0.08$ (Paper V), so that we expect that the mean effective mass-to-light ratio is 38% of the mean total mass-to-light ratio, on average. Second, we note that the maximum rotational velocities were not corrected for turbulent/z-motions by GPB, so that the estimates of the total mass-to-light ratios further exceed those of the effective mass-to-light ratio for the low-mass objects. We conclude that the two estimates are consistent within the assumptions and the uncertainties of the observations.

What do these two estimates tell us about the radial behaviour of the mass-to-light ratio? The mass of a spiral galaxy within a given galactocentric distance lays with high confidence between the estimates given by a flat disk model and a spherical one and is between 60 and 100% of the mass estimate determined through the assumption of spherical symmetry (Lequeux 1983). According to this author, the overestimate due to this assumption is probably much reduced at galactocentric distances as large as the optical radius, where spherical components dominate the potential. Hence, the 60% difference between the average estimates of the effective and total mass-to-light ratios may suggest that the actual mass-to-light ratio increases with galactocentric distance.

A linear fit to the data of all the galaxies later than S0a which minimizes the dispersion in both axes gives:

$$\kappa_3 = -0.076(\pm 0.021)\kappa_1 + 0.904(\pm 0.070). \quad (14)$$

Formally this relation corresponds to the scaling relations $M_e/L_e \propto M_e^{-0.093 \pm 0.026}$ and $M_e/L_e \propto L_e^{-0.103 \pm 0.032}$. The slight dependences of the effective mass-to-light ratio on effective mass and luminosity are marginally significant. We note that the adoption of velocity corrections for turbulent/z-motions gives us some protection against a systematic overestimate of the mass of the Scd–Im/BCD galaxies, where such motions are not negligible with respect to the rotational velocity. The incompleteness bias which affects our sample may justify even higher mass-to-light ratios for these galaxies, since we better observe low-mass objects of higher luminosity. On the other end, Lequeux (1983) shows

that the discrepancy between the estimates of the mass-to-light ratio given by a flat disk model and a spherical one depends on its rotation curve. In a disk where the rotation curve increases linearly until a radial distance a , where it reaches its maximum, and stays flat at larger radii, this assumption leads to a discrepancy increasing from 40 to 50% when a ranges between 0 and the optical radius. Since rotation curves seem to peak at larger radial distances with decreasing mass of the system (Persic, Salucci & Stel 1996), it is reasonable to assume that our estimates of the effective mass-to-light ratio for the Scd-Im/BCD galaxies may be systematically in excess by an additional 10% with respect to those of earlier and more massive late-types. Furthermore, setting the velocity at the effective radius equal to the maximum velocity may lead to an overestimate of the dynamical mass of these systems, as discussed in Sect. 2. Alternatively, the decrease of the dynamical mass-to-light ratio with mass may be attributed to increasing extinction, as an effect of the mass-metallicity relation (Zaritsky, Kennicutt & Huchra 1994). At present, there are no estimates of such an effect, obtained from modelling both kinematics and radiative transfer and we assume that these effects are very small in the near-IR. Hence, we conclude that the validity and interpretation of the scaling relations involved by Equ. 14 are dubious.

4.2 Galaxies in the κ_2 - κ_3 plane

4.2.1 Ellipticals and lenticulars

In this projection of the κ -space, the distribution of the E and S0 galaxies is elongated in the direction of the κ_2 axis, so that $I_e \propto (M_e/L_e)^{-3}$ for these objects (Fig. 2a). A similar distribution is found by PDdC and BBFN. Therefore, we conclude that the higher is the mass of an elliptical/lenticular galaxy the higher is its mean effective mass-to-light ratio and the lower is its effective surface intensity, whatever the pass-band is. S0a galaxies distribute in a similar way to the early-types.

4.2.2 Spirals and Im/BCDs

For the late-type galaxies, the coordinates κ_2 and κ_3 are not independent. As shown by BBFN, the distribution of the spiral and Im/BCD galaxies in this plane reproduces the generalized Tully-Fisher (TF) relation $\log L_T = A_C \log V_{Max} + \text{const.}$, where A_C is the color-dependent exponent in the standard TF power law. In the near-IR $A_C = 4$ (Aaronson et al. 1979) whatever the morphological type is (e.g. Pierini & Tuffs 1999) and, as a consequence, spiral and Im/BCD galaxies distribute in a plane that projects with minimal scatter onto κ_2 - κ_3 (BBFN). For the present sample of late-type galaxies we obtain $A_C = 3.851 \pm 0.074$, consistent with the standard exponent of the near-IR TF relation, but the scatter in the κ_2 - κ_3 plane is still large. We conclude that, whatever the astrophysical origin of the TF relation is (e.g. Silk 1997; Avila-Reese & Firmani 2000), its existence implies a non-linear relation between effective surface intensity and mass-to-light ratio along the whole Hubble sequence of the spiral galaxies (Pierini & Tuffs 1999). The exponent of this power law depends on the observing wavelength and is ~ 1.5 in the near-IR.

4.3 Galaxies in the κ_1 - κ_2 plane

4.3.1 Ellipticals and lenticulars

The κ_1 - κ_2 plane may be considered a sort of face-on projection of the galaxy distribution in the κ -space (BBFN), where early- and late-type galaxies distribute in two broad and almost perpendicular regions. Elliptical and lenticular galaxies populate the broad region defined by $\kappa_1 > 2.5$ and $\kappa_2 > 3$, with $\kappa_1 + \kappa_2 < 9$, approximately, together with the S0a galaxies. This result is consistent with the distribution of similar galaxies in PDdC and BBFN. In analogy with the latter authors we call “Zone of Exclusion” the region with $\kappa_1 + \kappa_2 \geq 9$.

4.3.2 Spirals and Im/BCDs

The galaxies with morphological type later than S0a populate a broad region defined by $-1 < \kappa_2 - \kappa_1 < 2$, with $\kappa_1 + \kappa_2 < 9$. Individual late-type galaxies distribute inside this strip and further away from the “Zone of Exclusion” according to the progression in morphological type from Sa to Im/BCD, as found in the optical (BBFN). Consistently, late-type galaxies with decreasing values of the light concentration index c_{31} populate regions further away from the “Zone of Exclusion”. By contrast, all our E+S0+S0a galaxies have $c_{31} > 2.82$, the typical value for a pure exponential disk-system, and do not show any relation between their location in the κ_1 - κ_2 plane and their value of c_{31} .

4.3.3 The “generalized” Kormendy relation

The similar behaviours of early- and late-type galaxies in the optical and near-IR κ_1 - κ_2 planes must reproduce a change in the relation between fundamental structural parameters, independent of the observational wavelength where these parameters are determined. As suggested by BBFN, the distribution of giant and dwarf early-type galaxies in the optical κ_1 - κ_2 plane is analogous to the division of these stellar systems found by Kormendy (1988), the behaviour of the Sa-Sc galaxies resembling that of the giant ellipticals and lenticulars.

Therefore, we plot μ_e vs. r_e for the pure de Vaucouleurs systems (filled hexagons) in Fig. 3a and for all the E+S0 galaxies of our sample (filled circles and empty squares, respectively) in Fig. 3b. The Kormendy relation (Kormendy 1977, 1988; Burstein 1979) of the E galaxies of the present sample is reproduced in each panel:

$$\mu_e = 2.65(\pm 0.07) \log r_e + 15.65(\pm 0.04). \quad (15)$$

It is no surprise that the subsample of the pure de Vaucouleurs systems follows such a relation, since this is a natural consequence of the $r^{1/4}$ law of their light profiles (Khosroshahi, Wadadekar & Kembhavi 2000). However, all the E+S0 galaxies distribute along the same mean relation (Fig. 3b), whatever their radial surface brightness profiles are. Hence we conclude that the Kormendy relation is not an artifact of the $r^{1/4}$ law but it expresses a unique property of all these stellar systems.

In addition, we plot μ_e vs. r_e for the pure exponential disk-systems plus the truncated-disk systems (empty triangles in Fig. 3c) and for all the de Vaucouleurs/exponential

bulge+exponential disk systems (filled squares in Fig. 3d). We find that the distribution of the late-type galaxies as a whole class in the near-IR $r_e-\mu_e$ plane is similar to the distribution of their disk-components in the near-IR and optical $h-\mu_0$ planes (Grosbøl 1985; de Jong 1996a; Dalcanton, Spergel & Summers 1997; Pierini 1997). In fact:

- the mean effective surface intensity of spiral systems as a whole and the central intensity of their exponential disk-components range within a broad but upper limited interval for any value of the effective radius and of the exponential disk scale-length, respectively;
- in both distributions the limiting intensity is constant for systems with characteristic sizes less than ~ 1 kpc, but decreases in systems of larger characteristic sizes.

It is interesting to realize that the Kormendy relation of the ellipticals represents the borderline of the broad region in the $r_e-\mu_e$ plane populated by the late-type galaxies. In particular, the bulge+disk late-type galaxies populate a strip parallel and immediately below the locus defined by the Kormendy relation, consistent with Khosroshahi et al. (2000), while the pure exponential/truncated disks populate the whole permitted region of the $r_e-\mu_e$ plane.

The comparison of Fig. 1 and 3 may suggest that structure changes with the mass of the stellar system (Paper V and IX), under the assumption of homologous classes of galaxies in gravitational equilibrium, and that this equilibrium holds only outside the “Zone of Exclusion” (BBFN).

5 DISCUSSION AND CONCLUSIONS

The existence of the Hubble sequence of galaxies (Hubble 1926; Sandage 1961) reflects differences in structure, kinematics and global star-formation histories of the classified stellar systems (Roberts & Haynes 1994). The study of the galaxy distribution in the so-called κ -space (BBFN) contributes to the understanding of the galaxy phenomenology, under the non trivial assumption that early- and late-type galaxies form two distinct homologous classes in gravitational equilibrium. Our investigation of the κ -space of nearby galaxies is based on near-IR surface photometry and is complementary to the near-IR studies of PDdC (limited to ellipticals and lenticulars) and Moriondo, Giovanelli & Haynes (1999) (limited to bulges and disks of late-type galaxies) and to the optical study of BBFN, though the photometric parameters are derived via different procedures in these four studies.

As a first result, we find that galaxies of the same morphological type distribute in the $\kappa_1-\kappa_2$ projection of the κ -space in a way analogous to the optical case. This distribution reproduces the “generalized” Kormendy relation (BBFN) since it finds analogies with the Kormendy relation of elliptical and lenticular galaxies (Kormendy 1977, 1988; Burstein 1979) on one hand and, on the other, the distribution of the disk-components of late-type galaxies in the $h-\mu_0$ plane (Grosbøl 1985; de Jong 1996a; Pierini 1997). It traces changes in the global structure associated with the dynamical mass of the galaxy (cf. Paper V and IX), beyond any possible systematic effect due to differences in the radial distribution of the stellar populations which dominate the light emission in different pass-bands, whether these differences

are intrinsic or due to differential attenuation by dust (cf. Witt, Thronson & Capuano 1992 for the early-type galaxies). We also confirm that the distribution of the early-type galaxies in the $\kappa_1-\kappa_3$ plane reproduces their Fundamental Plane relation and that, conversely, the distribution of the late-type galaxies in the $\kappa_2-\kappa_3$ plane reproduces the Tully–Fisher relation of the latter stellar systems. This time, the galaxy distribution in the $\kappa_1-\kappa_3$ and $\kappa_2-\kappa_3$ projections of the κ -space depends on the pass-band adopted in order to determine the photometric properties of the galaxies, as a consequence of the dominant role of the mass-to-light ratio.

The Fundamental Plane relation (in κ -space notation) shows that the dynamical mass-to-light ratio of elliptical and lenticular galaxies increases with dynamical mass, both in the optical and in the near-IR. The neglect of dust effects, even for rather modest amounts of dust, leads to an overestimate of the total dynamical mass-to-light ratio by a factor of $\sim 20\%$ per optical depth unit (Baes, Dejonghe & Rijkse 2000). Therefore, this relation holds almost unaffected by dust bias of the photometric properties in the near-IR. By contrast, the neglect of the rotational velocity on the mass estimate affects the Fundamental Plane relation, whatever the photometric pass-band is. We estimate that the systematic underestimate of the dynamical mass of the ellipticals is about 10%, on average. As a consequence, in the near-IR, a giant elliptical galaxy would have a corrected mean effective mass-to-light ratio of about 1.6 (in solar units), on average, still lower than the average mean effective mass-to-light ratio of late-type galaxies. The correction for the lenticular galaxies is not straightforward, but we may expect that it ranges between 10 and 30%, on average, the latter value applying to rotating ellipticals of maximum ellipticity ~ 0.4 . As a consequence, in the near-IR, the corrected mean effective mass-to-light ratios of lenticular galaxies might be intermediate between those of earlier and later Hubble types.

Spiral and Im/BCD galaxies show very different behaviours in the optical and near-IR $\kappa_1-\kappa_3$ planes. First of all, they have mean effective mass-to-light ratios higher than those of elliptical and lenticular galaxies of the same mass in the near-IR but it is vice versa in the optical (cf. BBFN). A study of the non-trivial effects of dust attenuation on the surface photometry of the late-type galaxies is beyond the reach of this analysis and, therefore, we have assumed statistically-based inclination corrections of the near-IR photometric parameters of these stellar systems (Equ. 10 and 11). In the near-IR, these corrections produce an increase of the mean effective mass-to-light ratio (Fig. 3a,b), opposite to what expected for early-type galaxies, so that we are confident that the relative distribution of early- and late-type galaxies $\kappa_1-\kappa_3$ plane is robust. Second, in the optical, the mass-to-light ratio vs. mass relation shows a strong dependence on the Hubble type of the spiral and Im/BCD galaxies. In the near-IR this dependence is not detected (if any) though there may be a hint that Im/BCD galaxies have higher mass-to-light ratios than spirals.

If not due to systematic differences either in the statistically-based corrections for dust effects and inclination adopted by us and BBFN or in the estimate of the photometric parameters, the different locations of early- and late-type galaxies in the optical and near-IR $\kappa_1-\kappa_3$ planes may originate from residual dust effects and/or from differences in the characteristic stellar populations, both dependent on

morphology and mass. The stellar mass-to-light ratio of a simple stellar population (SSP) increases with age both in the optical and in the near-IR, its early-time evolution being very fast until ~ 5 Gyrs and becoming mild afterwards (e.g. Maraston 1998). In particular, the stellar mass-to-near-IR light ratio reaches a value within 20% from the present one (~ 1.2 at 15 Gyrs) after only 3 Gyrs, while the stellar mass-to-optical light ratio amounts to 80% of the present one (~ 10) after 13 Gyrs. Of course a galaxy is not reproduced by a SSP but by a mix of different SSPs, weighted by its global star formation history. In particular, star formation activity leads to dust production, so that the mass-to-light ratio of a more recently born SSP will be reduced by dust attenuation both at the stellar photosphere and in the interstellar medium. It is commonly accepted that the bulk stellar population of giant elliptical and lenticular galaxies is older than those of spiral and Im/BCD galaxies, i.e. that the former have transformed gas into stars much faster than the latter (e.g. Renzini 1998). An analogous trend of decreasing ages of the characteristic stellar population with later Hubble type is suggested for the late-type galaxies (e.g. Sandage 1986; Kennicutt, Tamblyn & Congdon 1994; Gavazzi & Scodreggio 1996; Boselli et al. 2001). If these considerations apply, we expect that the early-type galaxies have higher stellar mass-to-light ratios than later ones, where star formation is still going on, under the assumptions that galaxies of all morphological types have the same age and the same initial mass function. In particular, the stellar mass-to-near-IR light ratios of nearby early- and late-type galaxies will not differ much if the peak of star formation activity took place more than 3 Gyrs ago for all of them. By contrast, the stellar mass-to-optical light ratios of early- and late-type galaxies may still differ by a maximum factor of ~ 7 (Maraston 1998), if this peak took place not less than 3 Gyrs ago for all of them.

We observe that the dynamical mass-to-near-IR light ratio of elliptical and lenticular galaxies is lower than that of spiral of the same dynamical mass. From the previous considerations, we conclude that the dynamical-to-stellar mass ratio of the former galaxies is lower than that of the latter, if the peak of the star formation activity took place more than 3 Gyrs ago for all of them. Extending the same conclusion to Im and BCD galaxies is dangerous, since the near-IR luminosity may be seriously contaminated by emission from younger stellar populations. Since BBFN observe that the dynamical mass-to-optical light ratio of elliptical and lenticular galaxies is higher than that of spiral galaxies of the same dynamical mass, this behaviour is consistent with the previous conclusion if the difference in the stellar mass-to-optical light ratio, due to the different star formation histories of these two classes of stellar systems, is larger than the difference in the dynamical-to-stellar mass ratio.

Finally, we note that the optical and near-IR Fundamental Plane relations should be analogous if the peak of star formation took place more than 3 Gyrs ago for all the elliptical and lenticular galaxies, but for a color term, when the differential effects of diffuse dust on the photometric parameters are taken into account. Whether this color term is not or is constant, it depends on the existence of the color-magnitude relation or not (Scodreggio 2001 and references therein). The answer to this question would help understanding whether the Fundamental Plane relation (in

κ -space notation) is (mainly) due to the increase either of the dynamical-to-stellar mass ratio or of the stellar mass-to-light ratio with dynamical mass.

ACKNOWLEDGMENTS

D.P. wishes to thank David C. Koo and Claudia S. Möller for illuminating discussions held at the Göttingen Sternwarte. We are thankful to the several night-assistants, undergraduate students and researchers who contributed to the near-IR survey at the basis of this work.

We are grateful to the anonymous referee, whose stimulating comments and suggestions led to the improvement of the original manuscript.

REFERENCES

- Aaronson M., Huchra J., Mould J., 1979, *ApJ*, 229, 1
- Avila-Reese V., Firmani C., 2000, in “The seventh Texas–Mexico conference on astrophysics: flows, blows, and glows”, (Eds.: W.H. Lee and S. Torres–Peimbert), *Rev. Mex. Astron. Astrofis. Serie de Conf. vol. 10*, p.97
- Baes M., Dejonghe H., 2000, *MNRAS*, 313, 153
- Baes M., Dejonghe H., De Rijcke S., 2000, *MNRAS*, 318, 798
- Bender R., Burstein D., Faber S.M., 1992, *ApJ*, 399, 462
- Bianchi S., Ferrara A., Davies J.I., Alton P.B., 2000, *MNRAS*, 311, 601
- Binggeli B., Sandage A., Tammann G.A., 1985, *AJ*, 90, 1681 (VCC)
- Binney J., Tremaine S., 1987, “Galactic dynamics”, Princeton University Press
- Bertola F., Galletta G., 1978, *ApJ*, 226, L115
- Boselli A., Gavazzi G., Donas J., Scodreggio M., 2001, *AJ*, 121, 753
- Boselli A., Gavazzi G., Franzetti P., Pierini D., Scodreggio M., 2000a, *A&AS*, 142, 73 (Paper IV)
- Boselli A., Tuffs R.J., Gavazzi G., Hippelein H., Pierini D., 1997, *A&AS*, 121, 507 (B97)
- Burstein D., 1979, *ApJ*, 234, 435
- Burstein D., Bender R., Faber S.M., Nolthenius R., 1995, *Astron. Lett. and Commun.*, 31, 95
- Burstein D., Bender R., Faber S.M., Nolthenius R., 1997, *AJ*, 114, 1365 (BBFN)
- Busarello G., Capaccioli M., Capozziello S., Longo G., Puddu E., 1997, *A&A*, 320, 415
- Caon N., Capaccioli M., D’Onofrio M., 1993, *MNRAS*, 265, 1013
- Capelato H.V., de Carvalho R.R., Carlberg R.G., 1995, *ApJ*, 451, 525
- Capelato H.V., de Carvalho R.R., Carlberg R.G., 1997, in “Galaxy Scaling Relations: Origins, Evolution and Applications”, (Eds.: L.N. da Costa and A. Renzini), Springer-Verlag, p.33
- Cardelli J.A., Clayton G.C., Mathis J.S., 1989, *ApJ*, 345, 245
- Dalcanton J.J., Spergel D.N., Summers F.J., 1997, *ApJ*, 482, 659
- de Jong R.S., 1996a, *A&A*, 313, 45
- de Jong R.S., 1996b, *A&A*, 313, 377
- de Vaucouleurs G., 1948, *Ann. d’Astrophys.*, 11, 247
- de Vaucouleurs G., 1959, *Hand. der Physik*, 53, 311
- de Vaucouleurs G., 1977, *ApJS*, 33, 211
- de Zeeuw T., Franx M., 1991, *ARA&A*, 29, 239
- Disney M.J., Davies J.I., Phillipps S., 1989, *MNRAS*, 239, 939
- Djorgovski S., Davis M., 1987, *ApJ*, 313, 59
- Dressler A., Lynden-Bell D., Burstein D., Davies R.L., Faber S.M., Terlevich R., Wegner G., 1987, *ApJ*, 313, 42
- Faber S.M., Jackson R.E., 1976, *ApJ*, 204, 668

- Ferrara A., Bianchi S., Cimatti A., Giovanardi C., 1999, *ApJS*, 123, 437
- Firmani C., Avila-Reese V., 2000, *MNRAS*, 315, 457
- Freeman K.C., 1970, *ApJ*, 160, 811
- Gavazzi G., Boselli A., 1996, *Astroph. Lett. & Comm.*, 35, 1
- Gavazzi G., Scodreggio M., 1996, *A&A*, 312, L29
- Gavazzi G., Pierini D., Boselli A., 1996a, *A&A*, 312, 397 (GPB)
- Gavazzi G., Pierini D., Boselli A., Tuffs R.J., 1996b, *A&AS*, 120, 489 (Paper I)
- Gavazzi G., Pierini D., Baffa C., Lisi F., Hunt L.K., Randone I., Boselli A., 1996c, *A&AS*, 120, 521 (Paper II)
- Gavazzi G., Boselli A., Scodreggio M., Pierini D., Belsole E., 1999, *MNRAS*, 304, 595
- Gavazzi G., Franzetti P., Scodreggio M., Boselli A., Pierini D., 2000b, *A&A*, 361, 863 (Paper V)
- Gavazzi G., Franzetti P., Scodreggio M., Boselli A., Pierini D., Baffa C., Lisi F., Hunt L.K., 2000a, *A&AS*, 142, 65 (Paper III)
- Gavazzi G., Zibetti S., Boselli A., Franzetti P., Scodreggio M., Martocchi S., 2001, *A&A*, 372, 29 (Paper VI)
- Geha M., Guhathakurta P., van der Marel R., 2001, *astro-ph/0107010*
- Graham A., Colless M., 1997, *MNRAS*, 287, 221
- Grosbøl P.J., 1985, *A&AS*, 60, 261
- Hawarden T.G., Longmore A.J., Tritton S.B., Elson R.A.W., Corwin H.G., 1981, *MNRAS*, 196, 747
- Haynes M.P., Giovanelli R., 1984, *AJ*, 89, 758
- Hubble E., 1926, *ApJ*, 64, 321
- Jura M., 1986, *ApJ*, 306, 483
- Kennicutt R.C., Tamblyn P., Congdon C.W., 1994, *ApJ*, 435, 22
- Khosroshahi H.G., Wadadekar Y., Kembhavi A., 2000, *ApJ*, 533, 162
- Khosroshahi H.G., Wadadekar Y., Kembhavi A., Mobasher B., 2000, *ApJ*, 531, L103
- King I.R., 1966, *AJ*, 71, 64
- Kormendy J., 1977, *ApJ*, 218, 333
- Kormendy J., 1988, in “Origin, Structure and Evolution of Galaxies”, IAU Symposium 127, (Ed.: L.Z. Fang), World Scientific, Singapore, p.252
- Lequeux J., 1983, *A&A*, 125, 394
- Mao S., Mo H.J., 1998, *MNRAS*, 296, 847
- Mao S., Mo H.J., White S.D.M., 1998, *MNRAS*, 297, L71
- Maraston C., 1998, *MNRAS*, 300, 872
- Mo H.J., Mao S., White S.D.M., 1998, *MNRAS*, 295, 319
- Mobasher B., Guzman R., Aragon-Salamanca A., Zepf S., 1999, *MNRAS*, 304, 225
- Moriondo G., Giovanelli R., Haynes M.P., 1999, *A&A*, 346, 415
- Moriondo G., Baffa C., Casertano S., Chincarini G., Gavazzi G., Giovanardi C., Hunt L.K., Pierini D., Sperandio M., Trinchieri G., 1999, *A&AS*, 137, 101
- Pahre M.A., 1999, *ApJS*, 124, 127
- Pahre M.A., de Carvalho R.R., Djorgovski S.G., 1998, *AJ*, 116, 1606
- Pahre M.A., Djorgovski S.G., de Carvalho R.R., 1998, *AJ*, 116, 1591 (PDdC)
- Pahre M.A., Djorgovski S.G., de Carvalho R.R., 1999, in “Star Formation in Early Type Galaxies”, ASP Conference Series 163, (Eds.: P. Carral and J. Cepa), p. 17
- Peletier R.F., Balcells M., Davies R.L., Andredakis Y., Vazdekis A., Burkert A., Prada F., 1999, *MNRAS*, 310, 703
- Persic M., Salucci P., Stel F., 1996, *MNRAS*, 281, 27
- Pierini D., 1997, Ph.D. thesis, Univ. of Milano
- Pierini D., Tuffs R.J., 1999, *A&A*, 343, 751
- Renzini A., 1998, in “The Young Universe: Galaxy Formation and Evolution at Intermediate and High Redshift”, (Eds.: S. D’Odorico, A. Fontana and E. Giallongo), ASP Conference Series 146, p.298
- Richter O.-G., Huchtmeier W.K., 1984, *A&A*, 132, 253
- Rix H.-W., Carollo M., Freeman K., 1999, *ApJ*, 513, L25
- Roberts M., Haynes M., 1994, *ARA&A*, 32, 115
- Rubin V.C., Burstein D., Ford W.K., Thonnard N., 1985, *ApJ*, 289, 91
- Saglia R.P., Bender R., Dressler A., 1993, *A&A*, 279, 75
- Sandage A., 1961, “The Hubble Atlas of Galaxies”, Carnegie Institute of Washington DC
- Sandage A., 1986, *A&A*, 161, 89
- Scodreggio M., 2001, *AJ*, 121, 2413
- Scodreggio M., Gavazzi G., 1993, *ApJ*, 409, 110
- Scodreggio M., Gavazzi G., Belsole E., Pierini D., Boselli A., 1998, *MNRAS*, 301, 1001 (S98)
- Scodreggio M., Gavazzi G., Franzetti P., Zibetti S., Boselli A., Pierini D., 2001, *A&A*, in press (Paper IX)
- Silk J., 1997, *ApJ*, 481, 703
- Simien F., Prugniel P., 2000, *A&AS*, 145, 263
- Syer D., Mao S., Mo H.J., 1999, *MNRAS*, 305, 357
- Tammann G.A., 1980, in “ESO/ESA Workshop on Dwarf Galaxies”, Knudsen, (Eds.: M. Tarenghi and K. Khar), p. 3
- Teerikorpi P., 1987, *A&A*, 173, 39
- Teerikorpi P., 1990, *A&A*, 234, 1
- Tully R.B., Fisher J.R., 1977, *A&A*, 54, 661
- Whitmore B.C., Kirshner R.P., 1981, *ApJ*, 250, 43
- Witt A.N., Thronson H.A., Capuano J.M., 1992, *ApJ*, 393, 611
- Zaritsky D., Kennicutt R., Huchra J., 1994, *ApJ*, 420, 87 ASP Conference Series 8, p.1
- Zwicky F., Herzog E., Karpowicz M., Kowal C., Wild P., 1961–1968, “Catalogue of Galaxies and Clusters of Galaxies”, vol. 6, Pasadena, C.I.T. (CGCG)

FIGURE CAPTIONS

Fig. 1: The three-dimensional fold-out of the κ -space, where $\kappa_1 \propto \log M$, $\kappa_2 \propto \log I_e^3 \times M/L$ and $\kappa_3 \propto \log M/L$. Here, we represent elliptical (E) and S0 galaxies with filled circles, S0a galaxies with asterisks and Sa – Im/BCD galaxies with empty circles. In each panel, we represent characteristic observational errors (crosses) and the expected increase of the three κ -coordinates of E and S0 galaxies when the kinetic energy of these stellar systems is not negligible. Late-type galaxies have higher values of M/L than earlier ones of the same mass, contrary to what found by BBFN in the optical.

Fig. 2: The three-dimensional fold-out of the κ -space for different groups of morphological types is reproduced. In particular, we represent: E, S0 and S0a galaxies with filled circles, empty squares and asterisks, respectively (a); Sa+Sab and Sb galaxies with broad crosses and empty hexagons, respectively (b); Sbc and Sc galaxies with filled triangles and empty circles, respectively (c); Scd, Sd and irregular/BCD galaxies with empty pentagons, stars and crosses, respectively, and generic peculiar and irregular galaxies with broad triangles (d). In each panel, we represent characteristic observational errors with crosses and we reproduce the Fundamental Plane relation (continuous line in the κ_1 – κ_3 plane), the borderline of the “Zone of Exclusion” (short-dashed line in the κ_1 – κ_2 plane) and the distribution of the E+S0 galaxies, within $\pm 1\sigma$ from the mean, in the κ_2 – κ_3 plane. For E and S0 galaxies, we represent also the expected increase of the three κ -coordinates when the kinetic energy of these stellar systems is not negligible. Galaxies of later Hubble type march farther away from the “Zone of Exclusion”, while spiral and irregular/BCD galaxies have higher mean effective dynamical mass-to-near-IR

light ratios than E+S0+S0a galaxies.

Fig. 3: The galaxy distribution in the $r_e-\mu_e$ plane, according to the decomposition of their radial light profiles or morphology. Here, we represent: pure de Vaucouleurs systems with filled hexagons (**a**); E and S0 galaxies with filled circles and empty squares, respectively (**b**); pure exponential disk-systems and truncated-disk systems with empty triangles (**c**); de Vaucouleurs/exponential bulge+disk systems with filled squares (**d**). In each panel, the short-dashed line reproduces the Kormendy relation (Equ. 15) for the de Vaucouleurs systems. E+S0 galaxies follow this relation, whatever their profile decompositions are. Conversely, pure exponential disk-systems and truncated-disk systems do not populate the region of the $r_e-\mu_e$ plane beyond this line. Bulge+disk systems populate the region of the $r_e-\mu_e$ plane immediately below this line.

This paper has been produced using the Royal Astronomical Society/Blackwell Science L^AT_EX style file.

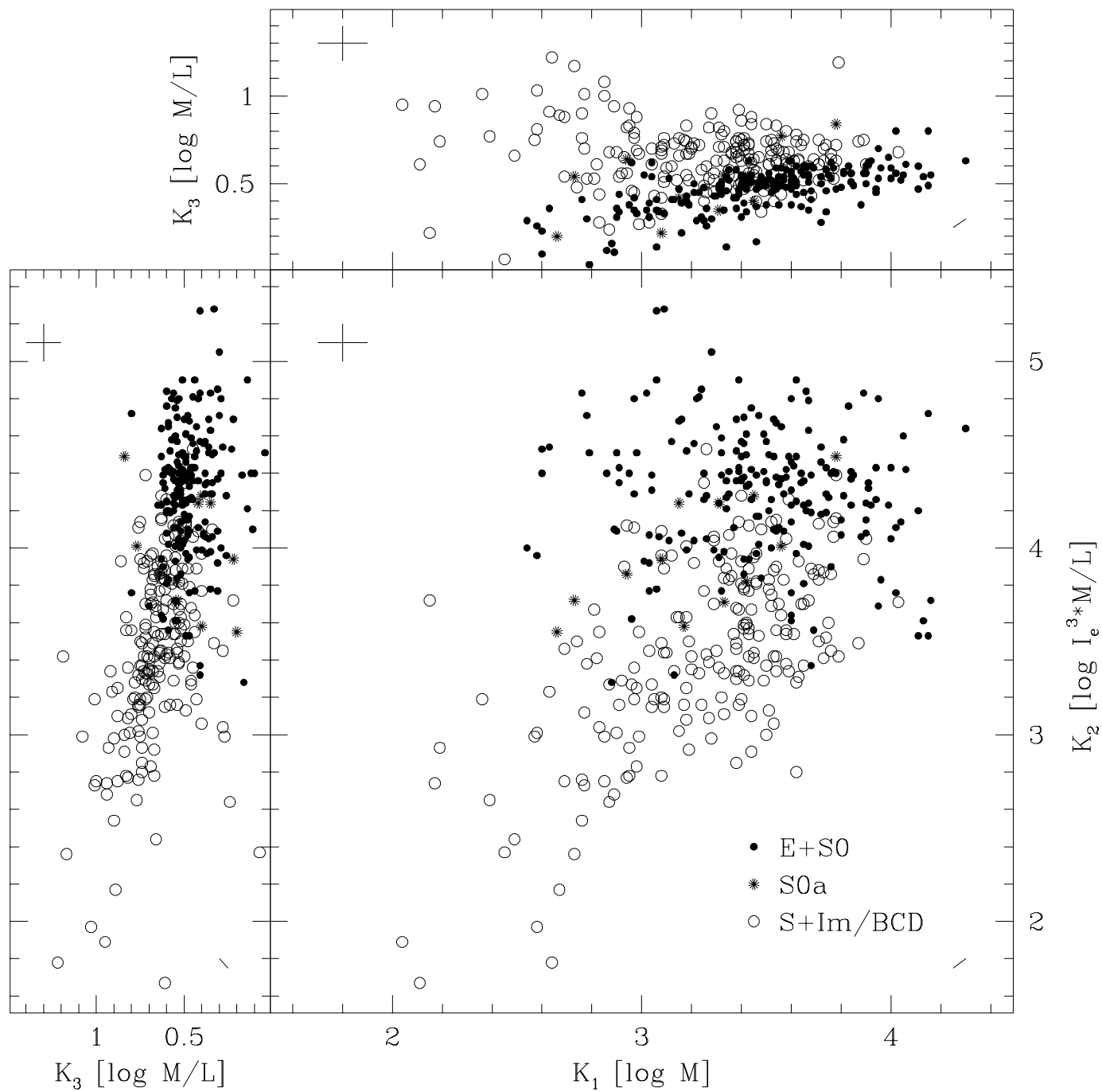


TABLE 1. Galaxy parameters

| Denomination CGCG / VCC | type | a /' | b /' | Dist. Mpc | log V km s ⁻¹ | μ_e mag arcsec ⁻² | log r _e kpc | κ_1 | κ_2 | κ_3 |
|----------------------------|------|---------|---------|--------------|-----------------------------|-------------------------------------|---------------------------|------------|------------|------------|
| CGCG 119024 | 1 | 1.74 | 0.87 | 62.6 | 2.50 | 16.74 | 0.45 | 3.64 | 4.40 | 0.57 |
| CGCG 119027 | 3 | 0.83 | 0.67 | 62.6 | 2.18 | 18.96 | 0.46 | 3.20 | 3.42 | 0.71 |
| CGCG 119028 | 13 | 0.97 | 0.47 | 28.4 | 1.98 | 20.79 | 0.26 | 2.77 | 2.73 | 1.01 |
| CGCG 119029 | 6 | 2.01 | 1.56 | 48.0 | 2.29 | 18.94 | 0.79 | 3.58 | 3.38 | 0.64 |
| CGCG 119031 | 1 | 1.61 | 0.89 | 62.6 | 2.43 | 17.51 | 0.64 | 3.67 | 4.01 | 0.55 |
| CGCG 119035 | 6 | 1.35 | 0.38 | 28.4 | 1.88 | 19.89 | 0.17 | 2.57 | 2.99 | 0.75 |
| CGCG 119044 | 13 | 0.93 | 0.41 | 48.0 | 1.90 | 21.01 | 0.40 | 2.76 | 2.54 | 0.90 |
| CGCG 119045 | 1 | 0.87 | 0.44 | 62.6 | 2.36 | 16.04 | 0.04 | 3.15 | 4.68 | 0.47 |
| CGCG 119046 | 7 | 1.85 | 1.19 | 48.0 | 2.17 | 19.08 | 0.49 | 3.20 | 3.35 | 0.70 |
| CGCG 119048 | 1 | 1.45 | 1.32 | 62.6 | 2.40 | 16.60 | 0.52 | 3.55 | 4.34 | 0.38 |
| CGCG 119050 | 4 | 1.78 | 1.18 | 62.6 | 2.42 | 17.80 | 0.60 | 3.63 | 3.93 | 0.63 |
| CGCG 119051 | 5 | 0.79 | 0.54 | 62.6 | 2.18 | 20.13 | 0.58 | 3.28 | 2.98 | 0.90 |
| CGCG 119053 | 2 | 0.63 | 0.50 | 62.6 | 2.16 | 17.96 | 0.13 | 2.94 | 3.86 | 0.64 |
| CGCG 119055 | 13 | 2.97 | 0.50 | 62.6 | 2.37 | 18.03 | 0.42 | 3.43 | 3.89 | 0.73 |
| CGCG 119058 | 1 | 1.71 | 0.46 | 62.6 | 2.48 | 16.61 | 0.54 | 3.68 | 4.39 | 0.46 |
| CGCG 119059 | 7 | 0.72 | 0.29 | 62.6 | 2.07 | 19.53 | 0.34 | 2.97 | 3.19 | 0.79 |
| CGCG 119063 | 2 | 1.09 | 0.75 | 62.6 | 2.64 | 16.96 | 0.35 | 3.78 | 4.49 | 0.84 |
| CGCG 119065 | 0 | 2.60 | 2.21 | 62.6 | 2.57 | 18.39 | 0.84 | 4.02 | 3.76 | 0.80 |
| CGCG 119066 | 5 | 1.06 | 0.75 | 56.4 | 2.20 | 18.46 | 0.37 | 3.15 | 3.63 | 0.66 |
| CGCG 119067 | 0 | 0.92 | 0.47 | 62.6 | 2.34 | 17.43 | 0.51 | 3.47 | 4.02 | 0.51 |
| CGCG 119068 | 3 | 0.99 | 0.73 | 84.4 | 2.34 | 17.78 | 0.36 | 3.36 | 3.97 | 0.68 |
| CGCG 119069 | 0 | 0.20 | 0.20 | 62.6 | 2.26 | 16.90 | 0.08 | 3.04 | 4.31 | 0.54 |
| CGCG 119070 | 7 | 1.28 | 0.42 | 48.0 | 1.99 | 20.80 | 0.41 | 2.89 | 2.68 | 0.94 |
| CGCG 119071 | 4 | 0.95 | 0.83 | 84.4 | 2.17 | 18.78 | 0.56 | 3.26 | 3.43 | 0.60 |
| CGCG 119072 | 0 | 0.93 | 0.93 | 84.4 | 2.30 | 17.12 | 0.46 | 3.37 | 4.11 | 0.42 |
| CGCG 119077 | 1 | 0.72 | 0.36 | 62.6 | 2.30 | 16.18 | 0.10 | 3.12 | 4.57 | 0.41 |
| CGCG 119078 | 7 | 2.41 | 1.67 | 28.4 | 2.29 | 18.66 | 0.54 | 3.41 | 3.57 | 0.72 |
| CGCG 119080W | 13 | 0.75 | 0.61 | 62.6 | 2.40 | 18.13 | 0.30 | 3.40 | 3.93 | 0.86 |
| CGCG 119080E | 13 | 1.40 | 0.54 | 62.6 | 2.14 | 18.52 | 0.53 | 3.19 | 3.50 | 0.52 |
| CGCG 119081 | 1 | 1.68 | 0.78 | 62.6 | 2.29 | 17.34 | 0.61 | 3.46 | 3.97 | 0.37 |
| CGCG 119083 | 5 | 2.67 | 0.55 | 62.6 | 2.38 | 18.18 | 0.73 | 3.67 | 3.72 | 0.60 |
| CGCG 119085 | 3 | 0.84 | 0.41 | 84.4 | 2.23 | 17.69 | 0.25 | 3.12 | 3.96 | 0.60 |
| CGCG 119092 | 12 | 1.33 | 0.42 | 62.6 | 2.10 | 19.39 | 0.46 | 3.08 | 3.20 | 0.71 |
| CGCG 119093 | 7 | 1.25 | 0.25 | 62.6 | 2.06 | 20.27 | 0.35 | 2.95 | 2.93 | 0.93 |
| CGCG 119096 | 7 | 1.28 | 0.34 | 113.2 | 2.29 | 19.08 | 0.78 | 3.59 | 3.34 | 0.68 |
| CGCG 119098 | 1 | 0.30 | 0.30 | 73.8 | 2.23 | 17.43 | 0.25 | 3.11 | 4.04 | 0.53 |
| CGCG 119101 | 1 | 0.74 | 0.37 | 62.6 | 2.09 | 16.11 | 0.16 | 2.86 | 4.40 | 0.12 |
| CGCG 97005 | 7 | 0.90 | 0.48 | 81.6 | 2.18 | 19.15 | 0.51 | 3.23 | 3.33 | 0.72 |
| CGCG 97021 | 0 | 0.60 | 0.60 | 88.6 | 2.25 | 16.55 | 0.41 | 3.26 | 4.28 | 0.26 |
| CGCG 127001 | 0 | 0.40 | 0.40 | 94.3 | 2.39 | 16.69 | 0.33 | 3.41 | 4.38 | 0.50 |
| CGCG 97023 | 1 | 0.73 | 0.71 | 84.4 | 2.31 | 16.92 | 0.28 | 3.25 | 4.26 | 0.48 |
| CGCG 97026 | 13 | 0.79 | 0.49 | 82.7 | 2.32 | 17.39 | 0.39 | 3.35 | 4.07 | 0.55 |
| CGCG 97027 | 7 | 0.95 | 0.63 | 88.4 | 2.25 | 18.77 | 0.57 | 3.38 | 3.49 | 0.68 |
| CGCG 127005 | 6 | 0.98 | 0.59 | 91.5 | 2.24 | 19.23 | 0.67 | 3.43 | 3.29 | 0.72 |
| CGCG 127023 | 0 | 0.70 | 0.70 | 89.1 | 2.38 | 16.96 | 0.40 | 3.44 | 4.26 | 0.51 |
| CGCG 157012 | 6 | 0.83 | 0.70 | 90.9 | 2.21 | 19.15 | 0.58 | 3.33 | 3.33 | 0.71 |
| CGCG 127025S | 6 | 1.39 | 0.87 | 94.4 | 2.23 | 18.07 | 0.62 | 3.38 | 3.68 | 0.46 |
| CGCG 127024 | 1 | 1.40 | 1.10 | 86.3 | 2.47 | 16.04 | 0.62 | 3.72 | 4.54 | 0.28 |
| CGCG 97055 | 0 | 0.40 | 0.30 | 86.6 | 2.43 | 16.65 | 0.36 | 3.49 | 4.41 | 0.52 |
| CGCG 97061 | 1 | 0.30 | 0.30 | 93.3 | 2.16 | 17.12 | 0.32 | 3.07 | 4.06 | 0.34 |
| CGCG 97063 | 13 | 0.58 | 0.34 | 86.6 | 1.97 | 18.78 | 0.28 | 2.78 | 3.38 | 0.53 |
| CGCG 97062 | 13 | 1.01 | 0.40 | 86.6 | 2.15 | 19.16 | 0.43 | 3.13 | 3.34 | 0.73 |
| CGCG 97068 | 6 | 1.23 | 0.76 | 86.6 | 2.33 | 17.16 | 0.43 | 3.39 | 4.14 | 0.49 |
| CGCG 127033 | 7 | 1.30 | 0.67 | 84.0 | 2.32 | 19.34 | 0.77 | 3.62 | 3.28 | 0.78 |
| CGCG 97072 | 3 | 1.21 | 0.54 | 86.6 | 2.22 | 18.48 | 0.62 | 3.37 | 3.54 | 0.55 |

TABLE 1. (continue)

| Denomination CGGC / VCC | type | a ' | b ' | Dist. Mpc | log V km s ⁻¹ | μ_e mag arcsec ⁻² | log r _e kpc | κ_1 | κ_2 | κ_3 |
|----------------------------|------|--------|--------|--------------|-----------------------------|-------------------------------------|---------------------------|------------|------------|------------|
| CGCG 97074 | 0 | 0.75 | 0.30 | 86.6 | 2.38 | 16.78 | 0.27 | 3.34 | 4.36 | 0.54 |
| CGCG 127035 | 3 | 1.20 | 0.30 | 90.9 | 2.36 | 18.36 | 0.60 | 3.55 | 3.70 | 0.69 |
| CGCG 97079 | 13 | 0.75 | 0.45 | 86.6 | 2.20 | 19.50 | 0.59 | 3.32 | 3.20 | 0.78 |
| CGCG 127037 | 13 | 0.80 | 0.45 | 82.5 | 2.10 | 19.57 | 0.46 | 3.09 | 3.15 | 0.76 |
| CGCG 127040 | 1 | 0.60 | 0.20 | 86.6 | 2.36 | 16.62 | 0.37 | 3.38 | 4.36 | 0.42 |
| CGCG 127038 | 7 | 1.91 | 1.55 | 92.2 | 2.14 | 19.24 | 1.02 | 3.53 | 3.06 | 0.40 |
| CGCG 97084 | 1 | 0.50 | 0.30 | 86.6 | 2.48 | 16.73 | 0.40 | 3.58 | 4.42 | 0.58 |
| CGCG 97087 | 13 | 2.00 | 0.50 | 86.6 | 2.48 | 17.47 | 0.66 | 3.77 | 4.06 | 0.59 |
| CGCG 97088 | 1 | 0.82 | 0.40 | 86.6 | 2.33 | 16.96 | 0.33 | 3.31 | 4.24 | 0.49 |
| CGCG 97090 | 1 | 0.62 | 0.45 | 86.6 | 2.39 | 16.44 | 0.21 | 3.32 | 4.51 | 0.51 |
| CGCG 97089 | 0 | 0.80 | 0.70 | 86.6 | 2.65 | 16.06 | 0.42 | 3.83 | 4.76 | 0.60 |
| CGCG 97091 | 3 | 1.12 | 0.81 | 86.6 | 2.25 | 18.32 | 0.64 | 3.42 | 3.60 | 0.53 |
| CGCG 97096 | 0 | 0.88 | 0.78 | 86.6 | 2.47 | 17.10 | 0.48 | 3.62 | 4.25 | 0.60 |
| CGCG 97095 | 0 | 1.95 | 1.59 | 86.6 | 2.63 | 17.21 | 0.84 | 4.11 | 4.20 | 0.60 |
| CGCG 97100 | 1 | 0.88 | 0.57 | 86.6 | 2.40 | 17.30 | 0.52 | 3.55 | 4.11 | 0.54 |
| CGCG 97102N | 3 | 1.08 | 0.65 | 86.6 | 2.29 | 18.32 | 0.58 | 3.44 | 3.67 | 0.62 |
| CGCG 97106 | 1 | 0.40 | 0.20 | 86.6 | 2.53 | 16.26 | 0.28 | 3.56 | 4.65 | 0.59 |
| CGCG 97112 | 1 | 0.60 | 0.20 | 86.6 | 2.29 | 15.67 | 0.19 | 3.16 | 4.69 | 0.22 |
| CGCG 97121 | 4 | 1.23 | 0.83 | 86.6 | 2.43 | 17.97 | 0.66 | 3.69 | 3.86 | 0.64 |
| CGCG 97117 | 1 | 0.90 | 0.50 | 86.6 | 2.48 | 17.23 | 0.55 | 3.68 | 4.19 | 0.60 |
| CGCG 97122 | 13 | 1.45 | 0.47 | 86.6 | 2.34 | 18.06 | 0.58 | 3.51 | 3.78 | 0.61 |
| CGCG 97124 | 0 | 0.20 | 0.20 | 86.6 | 2.36 | 16.90 | 0.32 | 3.35 | 4.29 | 0.52 |
| CGCG 97125 | 2 | 0.84 | 0.59 | 86.6 | 2.45 | 17.84 | 0.44 | 3.56 | 4.01 | 0.77 |
| CGCG 97127 | 0 | 1.62 | 1.58 | 86.6 | 2.56 | 16.80 | 0.61 | 3.84 | 4.37 | 0.56 |
| CGCG 97131 | 0 | 0.33 | 0.27 | 86.6 | 2.41 | 17.14 | 0.45 | 3.51 | 4.20 | 0.56 |
| CGCG 97134 | 1 | 1.31 | 0.44 | 86.6 | 2.50 | 18.32 | 1.13 | 4.13 | 3.61 | 0.54 |
| CGCG 97135 | 1 | 0.73 | 0.49 | 86.6 | 2.47 | 16.52 | 0.45 | 3.60 | 4.46 | 0.49 |
| CGCG 127048 | 0 | 0.50 | 0.50 | 90.9 | 2.60 | 15.90 | 0.27 | 3.66 | 4.84 | 0.60 |
| CGCG 97136 | 0 | 0.30 | 0.30 | 83.2 | 2.36 | 16.66 | 0.27 | 3.32 | 4.39 | 0.49 |
| CGCG 97137 | 0 | 0.90 | 0.80 | 86.6 | 2.53 | 16.70 | 0.56 | 3.76 | 4.40 | 0.53 |
| CGCG 127049 | 13 | 1.04 | 0.45 | 86.6 | 2.20 | 18.78 | 0.56 | 3.30 | 3.45 | 0.63 |
| CGCG 97143 | 0 | 0.30 | 0.20 | 86.6 | 2.04 | 16.70 | 0.31 | 2.89 | 4.10 | 0.11 |
| CGCG 127052 | 3 | 1.70 | 1.26 | 86.6 | 2.53 | 18.32 | 0.94 | 4.03 | 3.71 | 0.68 |
| CGCG 127053 | 6 | 1.40 | 0.50 | 85.5 | 2.21 | 20.27 | 0.99 | 3.62 | 2.80 | 0.74 |
| CGCG 97147 | 0 | 1.20 | 0.80 | 86.6 | 2.55 | 16.90 | 0.78 | 3.94 | 4.26 | 0.47 |
| CGCG 97152 | 3 | 1.20 | 0.38 | 86.6 | 2.29 | 18.61 | 0.53 | 3.41 | 3.59 | 0.72 |
| CGCG 97155 | 0 | 0.50 | 0.40 | 86.6 | 2.28 | 16.35 | 0.34 | 3.25 | 4.40 | 0.29 |
| CGCG 157035 | 5 | 2.12 | 1.57 | 83.7 | 2.52 | 17.33 | 0.61 | 3.78 | 4.16 | 0.63 |
| CGCG 127056 | 5 | 0.95 | 0.32 | 91.1 | 2.27 | 17.87 | 0.56 | 3.40 | 3.81 | 0.51 |
| CGCG 157037 | 0 | 0.40 | 0.40 | 89.5 | 2.23 | 17.15 | 0.45 | 3.26 | 4.05 | 0.36 |
| CGCG 127061 | 7 | 1.20 | 1.02 | 79.4 | 2.29 | 19.42 | 0.50 | 3.39 | 3.34 | 0.92 |
| CGCG 97161 | 0 | 0.90 | 0.90 | 83.3 | 2.60 | 16.38 | 0.50 | 3.81 | 4.58 | 0.57 |
| CGCG 157042 | 0 | 0.50 | 0.40 | 89.8 | 2.39 | 16.88 | 0.49 | 3.52 | 4.26 | 0.45 |
| CGCG 127071 | 13 | 0.76 | 0.46 | 90.9 | 2.00 | 18.91 | 0.49 | 2.96 | 3.27 | 0.46 |
| CGCG 127072 | 7 | 1.27 | 1.08 | 90.9 | 2.40 | 18.76 | 0.79 | 3.74 | 3.52 | 0.72 |
| CGCG 157044 | 13 | 0.70 | 0.30 | 88.1 | 2.53 | 19.66 | 0.60 | 3.79 | 3.42 | 1.19 |
| CGCG 127077 | 1 | 0.80 | 0.50 | 94.1 | 2.35 | 18.50 | 0.81 | 3.69 | 3.56 | 0.59 |
| CGCG 97169 | 7 | 1.00 | 0.20 | 79.7 | 2.24 | 19.24 | 0.50 | 3.31 | 3.36 | 0.82 |
| CGCG 127082 | 7 | 0.83 | 0.68 | 90.9 | 2.33 | 18.59 | 0.75 | 3.61 | 3.54 | 0.63 |
| CGCG 127088 | 0 | 1.82 | 1.59 | 90.9 | 2.64 | 16.73 | 0.68 | 4.00 | 4.43 | 0.59 |
| CGCG 127089 | 0 | 1.30 | 1.20 | 90.9 | 2.46 | 17.29 | 0.75 | 3.80 | 4.07 | 0.48 |
| CGCG 127092 | 0 | 0.50 | 0.50 | 90.9 | 2.32 | 17.86 | 0.58 | 3.48 | 3.84 | 0.54 |
| CGCG 127094 | 2 | 0.80 | 0.50 | 99.0 | 2.29 | 17.89 | 0.55 | 3.42 | 3.82 | 0.54 |
| CGCG 127099 | 7 | 1.34 | 0.67 | 86.0 | 2.35 | 17.79 | 0.59 | 3.53 | 3.88 | 0.55 |
| CGCG 98002 | 5 | 0.91 | 0.37 | 82.7 | 2.10 | 19.85 | 0.56 | 3.15 | 3.02 | 0.76 |

TABLE 1. (continue)

| Denomination CGCG / VCC | type | a ' | b ' | Dist. Mpc | log V km s ⁻¹ | μ_e mag arcsec ⁻² | log r _e kpc | κ_1 | κ_2 | κ_3 |
|----------------------------|------|--------|--------|--------------|-----------------------------|-------------------------------------|---------------------------|------------|------------|------------|
| CGCG 98007 | 6 | 0.90 | 0.38 | 84.6 | 2.23 | 19.24 | 0.62 | 3.38 | 3.30 | 0.74 |
| CGCG 157061 | 0 | 0.50 | 0.40 | 87.1 | 2.41 | 15.86 | 0.27 | 3.38 | 4.69 | 0.36 |
| CGCG 157062 | 13 | 1.10 | 0.26 | 91.8 | 1.92 | 20.57 | 0.27 | 2.69 | 2.75 | 0.88 |
| CGCG 157064 | 5 | 1.41 | 0.95 | 85.4 | 1.77 | 19.87 | 0.82 | 2.87 | 2.64 | 0.24 |
| CGCG 127115 | 1 | 1.50 | 1.10 | 85.8 | 2.59 | 16.97 | 0.64 | 3.91 | 4.32 | 0.61 |
| CGCG 127116 | 1 | 0.70 | 0.40 | 88.8 | 2.43 | 16.58 | 0.59 | 3.64 | 4.35 | 0.37 |
| CGCG 98013 | 7 | 0.89 | 0.49 | 92.7 | 2.28 | 18.63 | 0.64 | 3.47 | 3.53 | 0.65 |
| CGCG 127126 | 0 | 0.70 | 0.50 | 86.6 | 2.36 | 17.49 | 0.55 | 3.52 | 4.00 | 0.52 |
| CGCG 98016 | 7 | 1.38 | 0.43 | 86.0 | 2.21 | 19.57 | 0.67 | 3.39 | 3.16 | 0.76 |
| CGCG 157075 | 7 | 1.00 | 0.69 | 89.3 | 1.52 | 20.17 | 0.72 | 2.45 | 2.37 | 0.07 |
| CGCG 127130 | 0 | 0.50 | 0.50 | 99.8 | 2.46 | 16.99 | 0.57 | 3.67 | 4.24 | 0.51 |
| CGCG 98017 | 6 | 1.00 | 0.20 | 93.5 | 2.17 | 19.79 | 0.58 | 3.27 | 3.09 | 0.82 |
| CGCG 127135 | 2 | 0.60 | 0.35 | 92.1 | 2.11 | 18.19 | 0.55 | 3.17 | 3.58 | 0.40 |
| CGCG 127141 | 0 | 0.40 | 0.30 | 89.3 | 2.42 | 16.72 | 0.41 | 3.50 | 4.36 | 0.49 |
| CGCG 128003 | 13 | 0.97 | 0.72 | 85.8 | 2.37 | 18.80 | 0.62 | 3.58 | 3.56 | 0.80 |
| CGCG 98040 | 1 | 1.20 | 0.91 | 92.1 | 2.81 | 16.44 | 0.55 | 4.15 | 4.72 | 0.80 |
| CGCG 98042 | 0 | 1.82 | 1.48 | 92.1 | 2.55 | 16.66 | 0.65 | 3.85 | 4.39 | 0.49 |
| CGCG 98041 | 7 | 1.37 | 0.22 | 92.1 | 2.37 | 18.85 | 0.58 | 3.54 | 3.56 | 0.83 |
| CGCG 128009 | 0 | 1.20 | 1.20 | 92.1 | 2.23 | 16.52 | 0.56 | 3.34 | 4.21 | 0.14 |
| CGCG 98046 | 3 | 1.14 | 0.99 | 92.1 | 2.54 | 17.95 | 0.71 | 3.89 | 3.94 | 0.75 |
| CGCG 158010 | 6 | 0.80 | 0.40 | 105.7 | 2.31 | 17.95 | 0.57 | 3.46 | 3.81 | 0.57 |
| CGCG 98048 | 0 | 0.30 | 0.30 | 92.6 | 2.26 | 16.69 | 0.28 | 3.19 | 4.29 | 0.38 |
| CGCG 128021 | 6 | 1.20 | 0.20 | 94.2 | 2.36 | 18.25 | 0.56 | 3.52 | 3.75 | 0.69 |
| CGCG 98058 | 6 | 1.36 | 0.73 | 96.1 | 2.46 | 18.00 | 0.70 | 3.76 | 3.86 | 0.67 |
| CGCG 128034 | 0 | 0.87 | 0.83 | 90.9 | 2.43 | 16.13 | 0.39 | 3.50 | 4.57 | 0.38 |
| CGCG 128037 | 6 | 0.88 | 0.61 | 90.9 | 2.33 | 17.64 | 0.51 | 3.45 | 3.95 | 0.55 |
| CGCG 158038 | 4 | 0.92 | 0.54 | 89.7 | 2.31 | 18.15 | 0.52 | 3.43 | 3.77 | 0.64 |
| CGCG 98085 | 7 | 0.91 | 0.76 | 93.9 | 2.32 | 18.02 | 0.42 | 3.36 | 3.85 | 0.67 |
| CGCG 128053 | 6 | 1.56 | 0.49 | 97.4 | 2.25 | 18.88 | 0.65 | 3.43 | 3.42 | 0.67 |
| CGCG 128054 | 0 | 1.00 | 0.80 | 96.3 | 2.53 | 17.45 | 0.75 | 3.90 | 4.08 | 0.60 |
| CGCG 128059 | 5 | 1.00 | 0.65 | 89.8 | 2.28 | 17.94 | 0.47 | 3.35 | 3.83 | 0.58 |
| CGCG 98116 | 7 | 1.04 | 0.79 | 83.1 | 2.15 | 18.25 | 0.44 | 3.14 | 3.63 | 0.52 |
| CGCG 128063 | 3 | 2.12 | 0.85 | 90.0 | 2.38 | 17.84 | 0.56 | 3.54 | 3.90 | 0.62 |
| CGCG 158053N | 3 | 1.49 | 1.06 | 88.0 | 2.59 | 17.00 | 0.47 | 3.78 | 4.39 | 0.72 |
| CGCG 128065 | 0 | 1.70 | 1.70 | 89.8 | 2.56 | 17.07 | 0.70 | 3.90 | 4.24 | 0.56 |
| CGCG 128069 | 6 | 0.70 | 0.46 | 89.8 | 1.85 | 19.10 | 0.60 | 2.83 | 3.04 | 0.28 |
| CGCG 128073 | 5 | 1.53 | 0.77 | 92.7 | 2.23 | 18.79 | 0.72 | 3.45 | 3.41 | 0.58 |
| CGCG 158070 | 6 | 1.06 | 0.68 | 101.8 | 2.34 | 19.11 | 0.78 | 3.65 | 3.37 | 0.75 |
| CGCG 158097 | 1 | 0.60 | 0.30 | 98.0 | 2.24 | 17.29 | 0.53 | 3.33 | 3.98 | 0.35 |
| CGCG 128087 | 7 | 1.10 | 0.28 | 88.9 | 2.31 | 18.98 | 0.67 | 3.53 | 3.42 | 0.73 |
| CGCG 158105 | 6 | 1.20 | 0.57 | 91.0 | 2.33 | 18.33 | 0.61 | 3.52 | 3.69 | 0.66 |
| CGCG 158107 | 1 | 0.30 | 0.30 | 99.5 | 2.44 | 16.93 | 0.46 | 3.57 | 4.29 | 0.54 |
| CGCG 158106 | 0 | 0.40 | 0.30 | 92.5 | 2.48 | 15.55 | 0.14 | 3.39 | 4.90 | 0.44 |
| CGCG 128091 | 1 | 0.50 | 0.30 | 88.5 | 2.50 | 16.07 | 0.29 | 3.53 | 4.69 | 0.50 |
| CGCG 159005 | 6 | 1.27 | 0.73 | 93.3 | 2.24 | 18.65 | 0.82 | 3.54 | 3.42 | 0.50 |
| CGCG 159008 | 5 | 1.70 | 1.02 | 98.5 | 2.36 | 18.96 | 0.85 | 3.73 | 3.41 | 0.70 |
| CGCG 159010 | 5 | 1.30 | 0.33 | 93.5 | 2.25 | 18.81 | 0.67 | 3.45 | 3.44 | 0.64 |
| CGCG 129009 | 3 | 0.90 | 0.54 | 85.5 | 2.21 | 19.03 | 0.65 | 3.38 | 3.34 | 0.65 |
| CGCG 159021 | 0 | 1.40 | 1.10 | 89.3 | 2.68 | 16.31 | 0.67 | 4.05 | 4.60 | 0.55 |
| CGCG 159022 | 0 | 1.20 | 1.00 | 102.6 | 2.52 | 17.01 | 0.69 | 3.84 | 4.23 | 0.51 |
| CGCG 159031 | 3 | 1.30 | 0.59 | 100.1 | 2.28 | 17.40 | 0.38 | 3.29 | 4.04 | 0.52 |
| CGCG 159033 | 3 | 1.52 | 0.49 | 102.3 | 2.39 | 18.06 | 0.57 | 3.57 | 3.83 | 0.68 |
| CGCG 159037 | 4 | 0.86 | 0.58 | 97.3 | 2.31 | 18.57 | 0.73 | 3.58 | 3.54 | 0.61 |
| CGCG 159041 | 0 | 0.70 | 0.58 | 86.8 | 2.44 | 16.37 | 0.23 | 3.40 | 4.57 | 0.54 |
| CGCG 159043 | 0 | 0.78 | 0.57 | 89.3 | 2.57 | 15.94 | 0.26 | 3.60 | 4.80 | 0.57 |

TABLE 1. (continue)

| Denomination CGCG / VCC | type | a ' | b ' | Dist. Mpc | log V km s ⁻¹ | μ_e mag arcsec ⁻² | log r _e kpc | κ_1 | κ_2 | κ_3 |
|----------------------------|------|--------|--------|--------------|-----------------------------|-------------------------------------|---------------------------|------------|------------|------------|
| CGCG 159046 | 1 | 1.03 | 0.84 | 92.8 | 2.38 | 16.58 | 0.33 | 3.39 | 4.41 | 0.47 |
| CGCG 159055 | 6 | 1.40 | 0.31 | 103.2 | 2.19 | 19.70 | 0.63 | 3.33 | 3.11 | 0.80 |
| CGCG 159057 | 1 | 0.80 | 0.64 | 87.0 | 2.22 | 17.85 | 0.55 | 3.32 | 3.77 | 0.44 |
| CGCG 159058 | 3 | 0.90 | 0.44 | 90.6 | 2.30 | 17.39 | 0.60 | 3.46 | 3.97 | 0.40 |
| CGCG 159059 | 4 | 0.85 | 0.62 | 100.4 | 2.29 | 19.10 | 0.67 | 3.50 | 3.37 | 0.74 |
| CGCG 159063 | 1 | 0.65 | 0.62 | 100.6 | 2.34 | 16.87 | 0.35 | 3.34 | 4.27 | 0.46 |
| CGCG 100005 | 13 | 1.34 | 0.54 | 88.1 | 2.43 | 17.35 | 0.45 | 3.54 | 4.15 | 0.63 |
| CGCG 159070 | 1 | 1.28 | 1.04 | 93.2 | 2.50 | 15.96 | 0.50 | 3.67 | 4.63 | 0.35 |
| CGCG 100006 | 1 | 0.40 | 0.30 | 90.3 | 2.25 | 17.39 | 0.45 | 3.29 | 3.99 | 0.43 |
| CGCG 159075 | 2 | 0.87 | 0.52 | 88.1 | 2.28 | 16.77 | 0.41 | 3.31 | 4.24 | 0.35 |
| CGCG 159080 | 5 | 1.00 | 0.37 | 94.6 | 2.24 | 18.49 | 0.66 | 3.43 | 3.54 | 0.56 |
| CGCG 159082 | 7 | 1.11 | 0.72 | 107.7 | 2.29 | 19.08 | 0.85 | 3.63 | 3.31 | 0.64 |
| CGCG 159083 | 0 | 1.20 | 0.76 | 99.1 | 2.47 | 16.39 | 0.47 | 3.62 | 4.49 | 0.44 |
| CGCG 159085 | 1 | 1.82 | 1.38 | 92.0 | 2.50 | 18.39 | 0.89 | 3.95 | 3.69 | 0.70 |
| CGCG 159089 | 1 | 1.04 | 0.81 | 98.8 | 2.40 | 17.31 | 0.56 | 3.57 | 4.09 | 0.52 |
| CGCG 159090 | 7 | 0.81 | 0.58 | 110.9 | 1.89 | 19.21 | 0.74 | 2.99 | 2.99 | 0.27 |
| CGCG 159095 | 6 | 0.67 | 0.51 | 91.2 | 2.18 | 17.79 | 0.52 | 3.25 | 3.77 | 0.40 |
| CGCG 159096 | 7 | 1.67 | 0.62 | 82.5 | 2.20 | 20.18 | 0.77 | 3.44 | 2.91 | 0.84 |
| CGCG 159100 | 0 | 1.00 | 0.62 | 84.9 | 2.44 | 16.71 | 0.42 | 3.54 | 4.38 | 0.51 |
| CGCG 159101 | 13 | 0.44 | 0.36 | 92.0 | 2.12 | 18.63 | 0.28 | 2.99 | 3.55 | 0.67 |
| CGCG 160001 | 5 | 0.80 | 0.42 | 92.0 | 2.25 | 18.87 | 0.58 | 3.38 | 3.46 | 0.70 |
| CGCG 159105 | 0 | 1.12 | 0.91 | 93.4 | 2.47 | 17.20 | 0.53 | 3.66 | 4.20 | 0.59 |
| CGCG 160005 | 5 | 1.87 | 0.43 | 84.2 | 2.42 | 17.99 | 0.71 | 3.71 | 3.83 | 0.61 |
| CGCG 160008 | 1 | 1.94 | 1.44 | 92.0 | 2.58 | 17.21 | 0.87 | 4.04 | 4.14 | 0.52 |
| CGCG 160013 | 1 | 1.61 | 1.25 | 92.0 | 2.38 | 17.01 | 0.64 | 3.60 | 4.14 | 0.38 |
| CGCG 160017 | 0 | 0.99 | 0.70 | 92.0 | 2.51 | 16.99 | 0.60 | 3.75 | 4.27 | 0.55 |
| CGCG 160019 | 1 | 1.16 | 0.67 | 92.0 | 2.58 | 15.92 | 0.33 | 3.67 | 4.79 | 0.54 |
| CGCG 160021 | 1 | 2.04 | 1.41 | 92.0 | 2.50 | 17.95 | 0.90 | 3.96 | 3.83 | 0.59 |
| CGCG 160022 | 1 | 0.98 | 0.63 | 92.0 | 2.58 | 17.19 | 0.68 | 3.92 | 4.23 | 0.63 |
| CGCG 160023 | 0 | 0.65 | 0.59 | 92.0 | 2.42 | 16.62 | 0.34 | 3.44 | 4.42 | 0.51 |
| CGCG 160024 | 0 | 0.77 | 0.51 | 92.0 | 2.38 | 16.74 | 0.38 | 3.42 | 4.33 | 0.47 |
| CGCG 160026 | 7 | 0.85 | 0.55 | 92.0 | 2.24 | 20.00 | 0.77 | 3.50 | 3.00 | 0.84 |
| CGCG 160027 | 0 | 0.73 | 0.64 | 92.0 | 2.40 | 16.80 | 0.31 | 3.40 | 4.36 | 0.55 |
| CGCG 160028 | 1 | 1.50 | 1.16 | 92.0 | 2.61 | 17.21 | 0.72 | 3.99 | 4.23 | 0.65 |
| CGCG 160033 | 0 | 0.91 | 0.64 | 92.0 | 2.08 | 17.67 | 0.42 | 3.03 | 3.77 | 0.31 |
| CGCG 160037 | 1 | 0.61 | 0.58 | 92.0 | 2.53 | 16.23 | 0.26 | 3.54 | 4.67 | 0.59 |
| CGCG 160039 | 0 | 3.56 | 1.55 | 92.0 | 2.54 | 18.11 | 1.10 | 4.16 | 3.72 | 0.55 |
| CGCG 160041 | 2 | 1.17 | 0.41 | 92.0 | 2.24 | 18.13 | 0.52 | 3.33 | 3.71 | 0.55 |
| CGCG 160042 | 0 | 0.95 | 0.85 | 92.0 | 2.53 | 16.59 | 0.50 | 3.72 | 4.46 | 0.54 |
| CGCG 160044 | 0 | 1.59 | 1.55 | 92.0 | 2.57 | 17.34 | 0.84 | 4.02 | 4.11 | 0.56 |
| CGCG 160049 | 1 | 0.59 | 0.47 | 92.0 | 2.40 | 16.75 | 0.23 | 3.35 | 4.41 | 0.58 |
| CGCG 160058 | 6 | 1.24 | 0.42 | 92.0 | 2.15 | 18.75 | 0.62 | 3.27 | 3.39 | 0.53 |
| CGCG 160056S | 1 | 1.60 | 1.36 | 92.0 | 2.48 | 17.13 | 0.71 | 3.80 | 4.15 | 0.48 |
| CGCG 160062 | 0 | 0.85 | 0.49 | 92.0 | 2.26 | 18.63 | 0.99 | 3.68 | 3.37 | 0.41 |
| CGCG 160063 | 1 | 0.79 | 0.61 | 92.0 | 2.39 | 16.04 | 0.19 | 3.30 | 4.65 | 0.43 |
| CGCG 160065 | 0 | 0.90 | 0.82 | 92.0 | 2.42 | 16.77 | 0.40 | 3.50 | 4.35 | 0.52 |
| CGCG 160070 | 1 | 1.26 | 0.78 | 92.0 | 2.39 | 18.00 | 0.69 | 3.65 | 3.81 | 0.60 |
| CGCG 160071 | 1 | 1.51 | 0.89 | 92.0 | 2.49 | 16.61 | 0.43 | 3.61 | 4.44 | 0.53 |
| CGCG 160215 | 0 | 0.96 | 0.80 | 92.0 | 2.55 | 16.76 | 0.52 | 3.77 | 4.41 | 0.59 |
| CGCG 160217 | 0 | 0.74 | 0.64 | 92.0 | 2.32 | 16.31 | 0.16 | 3.18 | 4.52 | 0.43 |
| CGCG 160218 | 0 | 0.57 | 0.47 | 92.0 | 2.44 | 16.21 | 0.26 | 3.42 | 4.61 | 0.49 |
| CGCG 160219 | 1 | 0.58 | 0.48 | 92.0 | 2.39 | 16.20 | 0.21 | 3.32 | 4.59 | 0.46 |
| CGCG 160220 | 1 | 0.72 | 0.60 | 92.0 | 2.26 | 17.52 | 0.46 | 3.31 | 3.95 | 0.47 |
| CGCG 160221 | 0 | 1.51 | 0.81 | 92.0 | 2.43 | 17.02 | 0.52 | 3.60 | 4.23 | 0.51 |
| CGCG 160222 | 0 | 0.64 | 0.43 | 92.0 | 2.49 | 16.01 | 0.18 | 3.44 | 4.75 | 0.55 |

TABLE 1. (continue)

| Denomination CGCG / VCC | type | a ' | b ' | Dist. Mpc | log V km s ⁻¹ | μ_e mag arcsec ⁻² | log r _e kpc | κ_1 | κ_2 | κ_3 |
|----------------------------|------|--------|--------|--------------|-----------------------------|-------------------------------------|---------------------------|------------|------------|------------|
| CGCG 160224 | 0 | 1.02 | 0.57 | 92.0 | 2.52 | 16.61 | 0.61 | 3.78 | 4.40 | 0.47 |
| CGCG 160225 | 0 | 1.04 | 0.90 | 92.0 | 2.45 | 16.65 | 0.46 | 3.58 | 4.38 | 0.48 |
| CGCG 160227 | 1 | 0.65 | 0.57 | 92.0 | 2.38 | 17.23 | 0.54 | 3.53 | 4.10 | 0.48 |
| CGCG 160228 | 1 | 0.89 | 0.50 | 92.0 | 2.47 | 16.20 | 0.31 | 3.49 | 4.61 | 0.49 |
| CGCG 160229 | 1 | 0.57 | 0.49 | 92.0 | 2.33 | 17.91 | 0.74 | 3.60 | 3.76 | 0.47 |
| CGCG 160230 | 1 | 0.52 | 0.42 | 92.0 | 2.47 | 16.10 | 0.18 | 3.41 | 4.70 | 0.54 |
| CGCG 160231 | 0 | 2.27 | 1.93 | 92.0 | 2.46 | 18.38 | 1.19 | 4.11 | 3.53 | 0.47 |
| CGCG 160079 | 2 | 0.98 | 0.38 | 92.0 | 2.36 | 16.74 | 0.46 | 3.45 | 4.28 | 0.40 |
| CGCG 160234 | 0 | 0.61 | 0.52 | 92.0 | 2.41 | 16.47 | 0.28 | 3.40 | 4.49 | 0.50 |
| CGCG 160235 | 2 | 0.60 | 0.30 | 92.0 | 2.25 | 16.85 | 0.25 | 3.15 | 4.24 | 0.42 |
| CGCG 160237 | 1 | 0.61 | 0.57 | 92.0 | 2.38 | 16.53 | 0.32 | 3.39 | 4.43 | 0.46 |
| CGCG 160238 | 0 | 1.17 | 1.04 | 92.0 | 2.46 | 17.06 | 0.54 | 3.65 | 4.23 | 0.55 |
| CGCG 160239 | 0 | 0.54 | 0.50 | 92.0 | 2.32 | 18.35 | 0.76 | 3.60 | 3.61 | 0.55 |
| CGCG 160241 | 0 | 3.30 | 2.23 | 92.0 | 2.80 | 16.35 | 0.78 | 4.30 | 4.64 | 0.63 |
| CGCG 160242 | 0 | 0.40 | 0.30 | 92.0 | 2.17 | 17.16 | 0.25 | 3.03 | 4.07 | 0.39 |
| CGCG 160244 | 0 | 0.54 | 0.41 | 92.0 | 2.40 | 15.73 | 0.06 | 3.23 | 4.81 | 0.45 |
| CGCG 160246 | 0 | 0.58 | 0.43 | 92.0 | 2.35 | 16.24 | 0.15 | 3.21 | 4.56 | 0.45 |
| CGCG 160247 | 1 | 0.50 | 0.20 | 92.0 | 2.11 | 17.34 | 0.36 | 3.03 | 3.92 | 0.31 |
| CGCG 160248 | 0 | 0.85 | 0.62 | 92.0 | 2.46 | 17.86 | 0.71 | 3.76 | 3.90 | 0.62 |
| CGCG 160249 | 1 | 2.00 | 0.66 | 92.0 | 2.48 | 18.41 | 1.21 | 4.15 | 3.53 | 0.49 |
| CGCG 160250 | 1 | 0.82 | 0.49 | 92.0 | 2.30 | 17.78 | 0.53 | 3.41 | 3.86 | 0.52 |
| CGCG 160086 | 13 | 0.75 | 0.54 | 92.0 | 1.98 | 19.24 | 0.46 | 2.91 | 3.16 | 0.54 |
| CGCG 160251 | 2 | 0.60 | 0.20 | 92.0 | 2.11 | 17.18 | 0.44 | 3.08 | 3.94 | 0.22 |
| CGCG 160252 | 13 | 0.85 | 0.36 | 92.0 | 2.33 | 17.91 | 0.33 | 3.31 | 3.93 | 0.71 |
| CGCG 160088 | 5 | 1.12 | 0.64 | 92.0 | 2.37 | 18.78 | 0.88 | 3.76 | 3.45 | 0.64 |
| CGCG 160253 | 0 | 0.72 | 0.57 | 92.0 | 2.37 | 17.11 | 0.47 | 3.47 | 4.17 | 0.49 |
| CGCG 160254 | 0 | 0.70 | 0.48 | 92.0 | 2.21 | 17.14 | 0.34 | 3.16 | 4.08 | 0.39 |
| CGCG 160255 | 1 | 0.65 | 0.64 | 92.0 | 2.36 | 17.08 | 0.47 | 3.46 | 4.17 | 0.47 |
| CGCG 160256 | 0 | 0.84 | 0.64 | 92.0 | 2.48 | 15.99 | 0.25 | 3.47 | 4.71 | 0.48 |
| CGCG 160258 | 0 | 0.92 | 0.68 | 92.0 | 2.46 | 17.10 | 0.63 | 3.72 | 4.18 | 0.50 |
| CGCG 160259 | 0 | 1.49 | 0.98 | 92.0 | 2.49 | 17.19 | 0.60 | 3.74 | 4.19 | 0.58 |
| CGCG 160091 | 1 | 0.97 | 0.50 | 92.0 | 2.46 | 16.45 | 0.38 | 3.53 | 4.49 | 0.49 |
| CGCG 160092 | 0 | 0.40 | 0.40 | 92.0 | 2.35 | 17.78 | 0.46 | 3.43 | 3.94 | 0.63 |
| CGCG 160097 | 1 | 1.15 | 0.83 | 92.0 | 2.44 | 16.70 | 0.45 | 3.56 | 4.37 | 0.49 |
| CGCG 160099 | 1 | 1.32 | 0.65 | 92.0 | 2.54 | 17.40 | 0.87 | 4.00 | 4.05 | 0.53 |
| CGCG 160102 | 4 | 1.78 | 0.60 | 92.0 | 2.40 | 18.40 | 0.65 | 3.64 | 3.70 | 0.72 |
| CGCG 160100 | 0 | 0.72 | 0.67 | 92.0 | 2.43 | 16.52 | 0.21 | 3.38 | 4.52 | 0.58 |
| CGCG 160103 | 0 | 1.31 | 0.99 | 92.0 | 2.57 | 16.72 | 0.59 | 3.84 | 4.41 | 0.56 |
| CGCG 160105 | 1 | 1.07 | 0.74 | 92.0 | 2.60 | 16.93 | 0.63 | 3.91 | 4.35 | 0.62 |
| CGCG 160106 | 13 | 0.89 | 0.54 | 92.0 | 2.29 | 17.98 | 0.42 | 3.33 | 3.84 | 0.63 |
| CGCG 160113 | 0 | 0.96 | 0.80 | 92.0 | 2.43 | 17.55 | 0.60 | 3.65 | 4.02 | 0.59 |
| CGCG 160118 | 1 | 1.76 | 0.65 | 92.0 | 2.46 | 17.17 | 0.86 | 3.88 | 4.06 | 0.38 |
| CGCG 160121 | 5 | 1.40 | 0.44 | 92.0 | 2.28 | 18.38 | 0.52 | 3.39 | 3.67 | 0.66 |
| CGCG 160124 | 1 | 2.32 | 0.84 | 92.0 | 2.45 | 16.64 | 0.69 | 3.74 | 4.29 | 0.34 |
| CGCG 160123 | 0 | 0.82 | 0.59 | 92.0 | 2.40 | 16.82 | 0.35 | 3.43 | 4.34 | 0.53 |
| CGCG 130005 | 6 | 0.76 | 0.50 | 93.9 | 2.00 | 18.27 | 0.57 | 3.03 | 3.45 | 0.28 |
| CGCG 160127 | 7 | 0.95 | 0.64 | 92.0 | 2.07 | 19.92 | 0.68 | 3.19 | 2.92 | 0.67 |
| CGCG 160130 | 0 | 1.70 | 1.32 | 92.0 | 2.53 | 16.98 | 0.62 | 3.81 | 4.28 | 0.56 |
| CGCG 130008 | 7 | 0.57 | 0.49 | 96.9 | 2.30 | 17.87 | 0.58 | 3.46 | 3.82 | 0.53 |
| CGCG 160137 | 3 | 1.33 | 0.68 | 92.0 | 2.39 | 17.38 | 0.59 | 3.58 | 4.05 | 0.51 |
| CGCG 130009 | 6 | 1.44 | 0.87 | 84.5 | 2.19 | 18.87 | 0.86 | 3.49 | 3.29 | 0.46 |
| CGCG 160145 | 0 | 0.96 | 0.55 | 103.1 | 2.52 | 16.66 | 0.34 | 3.59 | 4.49 | 0.63 |
| CGCG 130012 | 6 | 1.83 | 0.43 | 95.1 | 2.44 | 17.90 | 0.70 | 3.73 | 3.87 | 0.63 |
| CGCG 130014 | 6 | 0.92 | 0.70 | 94.7 | 2.24 | 18.31 | 0.66 | 3.42 | 3.59 | 0.50 |
| CGCG 160156 | 3 | 1.56 | 0.94 | 96.8 | 2.34 | 18.11 | 0.77 | 3.65 | 3.70 | 0.52 |

TABLE 1. (continue)

| Denomination CGCG / VCC | type | a ' | b ' | Dist. Mpc | log V km s ⁻¹ | μ_e mag arcsec ⁻² | log r _e kpc | κ_1 | κ_2 | κ_3 |
|----------------------------|------|--------|--------|--------------|-----------------------------|-------------------------------------|---------------------------|------------|------------|------------|
| CGCG 160157 | 1 | 1.69 | 1.25 | 92.8 | 2.52 | 17.15 | 0.78 | 3.90 | 4.15 | 0.50 |
| CGCG 160158 | 1 | 1.44 | 1.00 | 93.8 | 2.38 | 17.52 | 0.66 | 3.62 | 3.97 | 0.49 |
| CGCG 130021 | 3 | 0.97 | 0.75 | 95.6 | 2.27 | 17.27 | 0.41 | 3.29 | 4.06 | 0.45 |
| CGCG 160168 | 7 | 1.39 | 1.18 | 99.7 | 2.43 | 17.87 | 0.69 | 3.71 | 3.88 | 0.61 |
| CGCG 130025 | 3 | 1.30 | 1.03 | 93.3 | 2.44 | 18.84 | 0.89 | 3.87 | 3.49 | 0.74 |
| CGCG 130027 | 6 | 1.17 | 0.32 | 91.1 | 2.29 | 17.97 | 0.25 | 3.21 | 3.92 | 0.73 |
| CGCG 160182 | 4 | 1.27 | 0.67 | 93.3 | 2.34 | 17.22 | 0.46 | 3.43 | 4.12 | 0.49 |
| CGCG 130030 | 0 | 1.00 | 1.00 | 92.8 | 2.46 | 16.67 | 0.54 | 3.65 | 4.36 | 0.45 |
| CGCG 160197 | 0 | 1.02 | 0.76 | 93.6 | 2.30 | 17.56 | 0.53 | 3.41 | 3.94 | 0.48 |
| CGCG 160209 | 13 | 0.85 | 0.57 | 95.6 | 2.00 | 19.02 | 0.61 | 3.05 | 3.19 | 0.43 |
| CGCG 101033 | 7 | 1.20 | 0.20 | 89.7 | 2.25 | 19.85 | 0.66 | 3.44 | 3.10 | 0.88 |
| CGCG 161040 | 7 | 0.74 | 0.40 | 96.8 | 2.00 | 20.21 | 0.66 | 3.08 | 2.78 | 0.67 |
| CGCG 101049 | 6 | 1.15 | 0.91 | 95.3 | 2.39 | 18.84 | 0.77 | 3.71 | 3.50 | 0.75 |
| CGCG 131008 | 6 | 1.20 | 0.20 | 79.5 | 2.33 | 18.20 | 0.47 | 3.41 | 3.78 | 0.69 |
| CGCG 161063 | 6 | 1.30 | 0.75 | 95.2 | 2.25 | 19.23 | 0.61 | 3.41 | 3.32 | 0.76 |
| CGCG 161069 | 5 | 0.90 | 0.77 | 95.6 | 2.46 | 17.08 | 0.45 | 3.59 | 4.26 | 0.60 |
| CGCG 161070 | 1 | 1.00 | 0.90 | 98.9 | 2.38 | 17.24 | 0.56 | 3.54 | 4.09 | 0.47 |
| CGCG 161073 | 5 | 1.92 | 0.82 | 97.6 | 2.53 | 17.53 | 0.75 | 3.90 | 4.05 | 0.61 |
| VCC 17 | 12 | 0.91 | 0.45 | 32.0 | 1.41 | 22.38 | 0.45 | 2.11 | 1.67 | 0.61 |
| VCC 58 | 5 | 3.16 | 2.19 | 32.0 | 2.22 | 19.49 | 0.67 | 3.40 | 3.19 | 0.75 |
| VCC 66 | 7 | 6.61 | 2.34 | 17.0 | 2.14 | 20.16 | 0.80 | 3.38 | 2.85 | 0.74 |
| VCC 73 | 5 | 2.14 | 0.79 | 32.0 | 2.33 | 16.75 | 0.24 | 3.25 | 4.35 | 0.49 |
| VCC 81 | 7 | 0.95 | 0.81 | 17.0 | 1.93 | 21.78 | 0.29 | 2.73 | 2.36 | 1.17 |
| VCC 87 | 11 | 1.82 | 0.91 | 17.0 | 1.75 | 20.68 | -0.13 | 2.17 | 2.74 | 0.94 |
| VCC 92 | 5 | 12.02 | 3.24 | 17.0 | 2.37 | 18.36 | 0.87 | 3.75 | 3.60 | 0.55 |
| VCC 120 | 8 | 4.47 | 0.81 | 32.0 | 2.13 | 19.25 | 0.54 | 3.18 | 3.25 | 0.67 |
| VCC 122 | 1 | 2.14 | 1.07 | 32.0 | 2.05 | 18.73 | 0.62 | 3.13 | 3.32 | 0.41 |
| VCC 145 | 7 | 6.31 | 1.07 | 17.0 | 2.13 | 19.55 | 0.52 | 3.17 | 3.16 | 0.75 |
| VCC 166 | 1 | 2.69 | 0.72 | 32.0 | 2.33 | 16.43 | 0.44 | 3.40 | 4.37 | 0.31 |
| VCC 220 | 1 | 3.39 | 1.07 | 32.0 | 2.46 | 16.49 | 0.34 | 3.51 | 4.50 | 0.53 |
| VCC 318 | 8 | 2.14 | 1.26 | 32.0 | 2.01 | 20.74 | 0.32 | 2.85 | 2.75 | 1.00 |
| VCC 345 | 0 | 4.90 | 3.63 | 32.0 | 2.66 | 16.77 | 0.72 | 4.06 | 4.42 | 0.61 |
| VCC 355 | 1 | 2.09 | 1.82 | 17.0 | 2.42 | 14.74 | -0.22 | 3.06 | 5.27 | 0.41 |
| VCC 382 | 7 | 2.51 | 1.62 | 32.0 | 2.26 | 17.66 | 0.49 | 3.34 | 3.89 | 0.48 |
| VCC 462 | 2 | 2.14 | 1.62 | 17.0 | 1.87 | 17.96 | 0.32 | 2.66 | 3.55 | 0.20 |
| VCC 497 | 7 | 8.32 | 2.00 | 17.0 | 2.26 | 17.85 | 0.59 | 3.41 | 3.79 | 0.47 |
| VCC 559 | 4 | 6.31 | 1.55 | 17.0 | 2.01 | 18.69 | 0.47 | 2.97 | 3.36 | 0.45 |
| VCC 613 | 3 | 4.37 | 1.26 | 17.0 | 2.19 | 17.30 | 0.08 | 2.94 | 4.12 | 0.56 |
| VCC 654 | 1 | 4.47 | 2.34 | 17.0 | 2.20 | 17.33 | 0.39 | 3.18 | 3.99 | 0.40 |
| VCC 685 | 1 | 3.98 | 1.45 | 17.0 | 2.43 | 15.04 | 0.09 | 3.28 | 5.05 | 0.30 |
| VCC 778 | 1 | 2.69 | 1.78 | 17.0 | 2.30 | 15.72 | -0.10 | 2.97 | 4.80 | 0.42 |
| VCC 784 | 1 | 2.69 | 2.00 | 17.0 | 2.00 | 16.08 | -0.01 | 2.60 | 4.40 | 0.10 |
| VCC 785 | 3 | 3.80 | 3.09 | 17.0 | 2.45 | 17.54 | 0.37 | 3.52 | 4.14 | 0.75 |
| VCC 787 | 8 | 2.00 | 1.17 | 23.0 | 1.99 | 19.75 | 0.43 | 2.90 | 3.01 | 0.68 |
| VCC 792 | 4 | 4.37 | 2.19 | 23.0 | 2.28 | 19.10 | 0.74 | 3.54 | 3.34 | 0.70 |
| VCC 828 | 0 | 2.00 | 0.91 | 17.0 | 2.20 | 16.22 | 0.00 | 2.90 | 4.51 | 0.36 |
| VCC 848 | 16 | 1.75 | 1.49 | 23.0 | 2.08 | 20.35 | 0.17 | 2.85 | 2.99 | 1.08 |
| VCC 849 | 6 | 2.18 | 1.82 | 23.0 | 2.09 | 19.25 | 0.41 | 3.04 | 3.27 | 0.70 |
| VCC 865 | 7 | 4.17 | 1.26 | 17.0 | 1.98 | 20.13 | 0.55 | 2.98 | 2.83 | 0.69 |
| VCC 873 | 7 | 4.90 | 1.45 | 17.0 | 2.04 | 18.26 | 0.56 | 3.08 | 3.49 | 0.33 |
| VCC 912 | 6 | 3.63 | 2.19 | 17.0 | 2.02 | 18.83 | 0.24 | 2.82 | 3.41 | 0.61 |
| VCC 921 | 6 | 2.14 | 1.78 | 17.0 | 2.03 | 19.22 | 0.30 | 2.87 | 3.27 | 0.68 |
| VCC 957 | 7 | 2.51 | 1.07 | 17.0 | 2.04 | 18.19 | 0.19 | 2.81 | 3.67 | 0.53 |
| VCC 958 | 3 | 4.37 | 1.74 | 17.0 | 2.36 | 16.31 | 0.19 | 3.26 | 4.53 | 0.45 |
| VCC 966 | 1 | 4.27 | 2.34 | 17.0 | 2.10 | 17.69 | 0.42 | 3.06 | 3.78 | 0.35 |

TABLE 1. (continue)

| Denomination CGGC / VCC | type | a ' | b ' | Dist. Mpc | log V km s ⁻¹ | μ_e mag arcsec ⁻² | log r _e kpc | κ_1 | κ_2 | κ_3 |
|----------------------------|------|--------|--------|--------------|-----------------------------|-------------------------------------|---------------------------|------------|------------|------------|
| VCC 971 | 9 | 3.80 | 0.54 | 23.0 | 1.91 | 20.38 | 0.38 | 2.76 | 2.76 | 0.76 |
| VCC 1025 | 0 | 1.75 | 1.75 | 17.0 | 2.21 | 16.49 | 0.00 | 2.91 | 4.43 | 0.44 |
| VCC 1030 | 1 | 3.63 | 3.09 | 17.0 | 2.38 | 16.22 | 0.38 | 3.42 | 4.50 | 0.34 |
| VCC 1047 | 3 | 2.51 | 2.14 | 17.0 | 2.19 | 17.17 | 0.27 | 3.08 | 4.09 | 0.42 |
| VCC 1126 | 7 | 3.63 | 1.45 | 17.0 | 2.00 | 18.29 | 0.30 | 2.83 | 3.55 | 0.44 |
| VCC 1146 | 0 | 1.97 | 1.67 | 17.0 | 2.18 | 17.67 | 0.21 | 3.01 | 3.93 | 0.55 |
| VCC 1154 | 1 | 4.17 | 3.24 | 17.0 | 2.40 | 16.16 | 0.33 | 3.41 | 4.56 | 0.39 |
| VCC 1178 | 0 | 1.63 | 1.15 | 17.0 | 2.23 | 15.64 | -0.26 | 2.76 | 4.83 | 0.41 |
| VCC 1190 | 3 | 5.37 | 1.62 | 23.0 | 2.35 | 17.98 | 0.57 | 3.51 | 3.83 | 0.61 |
| VCC 1196 | 2 | 1.94 | 1.17 | 17.0 | 2.03 | 18.10 | 0.10 | 2.73 | 3.72 | 0.54 |
| VCC 1242 | 1 | 3.09 | 1.45 | 17.0 | 2.22 | 16.17 | 0.07 | 2.98 | 4.51 | 0.33 |
| VCC 1250 | 1 | 2.14 | 1.07 | 17.0 | 2.06 | 16.00 | -0.14 | 2.60 | 4.53 | 0.23 |
| VCC 1279 | 0 | 2.14 | 1.62 | 17.0 | 2.31 | 15.55 | -0.04 | 3.02 | 4.83 | 0.35 |
| VCC 1290 | 5 | 2.51 | 1.35 | 17.0 | 2.25 | 18.69 | 0.29 | 3.18 | 3.63 | 0.83 |
| VCC 1303 | 1 | 2.34 | 0.91 | 23.0 | 2.18 | 16.66 | 0.15 | 2.97 | 4.29 | 0.35 |
| VCC 1316 | 0 | 11.00 | 11.00 | 17.0 | 2.67 | 15.85 | 0.46 | 3.89 | 4.83 | 0.56 |
| VCC 1318 | 1 | 6.31 | 2.19 | 17.0 | 1.88 | 18.45 | 0.61 | 2.88 | 3.28 | 0.16 |
| VCC 1321 | 1 | 2.00 | 1.74 | 17.0 | 1.94 | 17.20 | 0.06 | 2.58 | 3.96 | 0.26 |
| VCC 1356 | 15 | 1.31 | 0.51 | 17.0 | 1.93 | 19.85 | -0.22 | 2.36 | 3.19 | 1.01 |
| VCC 1375 | 7 | 5.89 | 4.68 | 17.0 | 2.12 | 19.54 | 0.27 | 2.98 | 3.25 | 0.88 |
| VCC 1379 | 7 | 3.55 | 1.91 | 17.0 | 2.04 | 19.35 | 0.51 | 3.04 | 3.15 | 0.61 |
| VCC 1401 | 6 | 8.91 | 4.79 | 17.0 | 2.48 | 17.22 | 0.67 | 3.77 | 4.14 | 0.53 |
| VCC 1410 | 11 | 1.69 | 0.90 | 17.0 | 2.00 | 19.64 | 0.01 | 2.63 | 3.23 | 0.91 |
| VCC 1450 | 7 | 3.24 | 2.51 | 17.0 | 1.96 | 19.55 | 0.28 | 2.77 | 3.12 | 0.70 |
| VCC 1475 | 0 | 1.63 | 1.15 | 17.0 | 2.11 | 16.17 | -0.20 | 2.63 | 4.54 | 0.36 |
| VCC 1508 | 7 | 4.47 | 3.24 | 17.0 | 2.10 | 19.44 | 0.47 | 3.09 | 3.19 | 0.72 |
| VCC 1535 | 1 | 7.00 | 2.01 | 17.0 | 2.58 | 16.52 | 0.72 | 3.94 | 4.43 | 0.45 |
| VCC 1537 | 1 | 2.14 | 0.89 | 17.0 | 2.18 | 15.73 | -0.13 | 2.78 | 4.71 | 0.30 |
| VCC 1615 | 5 | 7.41 | 6.17 | 17.0 | 2.28 | 18.11 | 0.78 | 3.56 | 3.64 | 0.44 |
| VCC 1619 | 0 | 4.90 | 1.10 | 17.0 | 2.07 | 15.76 | 0.10 | 2.79 | 4.51 | 0.04 |
| VCC 1630 | 0 | 2.51 | 2.00 | 17.0 | 2.20 | 16.48 | 0.07 | 2.95 | 4.40 | 0.38 |
| VCC 1632 | 1 | 8.91 | 8.91 | 17.0 | 2.58 | 15.64 | 0.26 | 3.62 | 4.90 | 0.51 |
| VCC 1664 | 0 | 5.37 | 1.62 | 17.0 | 2.35 | 15.53 | 0.15 | 3.22 | 4.80 | 0.29 |
| VCC 1690 | 4 | 13.18 | 6.61 | 17.0 | 2.37 | 17.59 | 0.77 | 3.68 | 3.89 | 0.43 |
| VCC 1699 | 11 | 1.75 | 0.94 | 17.0 | 1.76 | 20.61 | 0.17 | 2.39 | 2.65 | 0.77 |
| VCC 1720 | 1 | 4.68 | 3.24 | 17.0 | 2.25 | 17.38 | 0.34 | 3.21 | 4.04 | 0.50 |
| VCC 1725 | 15 | 1.75 | 1.10 | 17.0 | 1.72 | 20.87 | 0.38 | 2.49 | 2.44 | 0.66 |
| VCC 1726 | 10 | 1.85 | 1.44 | 17.0 | 1.76 | 22.36 | 0.43 | 2.58 | 1.97 | 1.03 |
| VCC 1727 | 4 | 7.76 | 6.03 | 17.0 | 2.45 | 17.23 | 0.64 | 3.71 | 4.13 | 0.52 |
| VCC 1758 | 7 | 2.14 | 0.35 | 17.0 | 1.91 | 19.93 | 0.13 | 2.58 | 3.01 | 0.81 |
| VCC 1760 | 3 | 5.37 | 1.45 | 17.0 | 2.10 | 18.67 | 0.48 | 3.09 | 3.44 | 0.54 |
| VCC 1789 | 12 | 1.31 | 0.73 | 17.0 | 1.73 | 19.99 | -0.07 | 2.19 | 2.93 | 0.74 |
| VCC 1791 | 15 | 1.85 | 0.92 | 17.0 | 1.79 | 21.77 | 0.49 | 2.67 | 2.17 | 0.89 |
| VCC 1811 | 7 | 2.69 | 1.78 | 17.0 | 1.96 | 18.64 | 0.18 | 2.69 | 3.46 | 0.54 |
| VCC 1813 | 3 | 5.89 | 5.01 | 17.0 | 2.31 | 17.03 | 0.60 | 3.48 | 4.10 | 0.34 |
| VCC 1827 | 1 | 1.85 | 1.22 | 17.0 | 2.11 | 18.41 | 0.26 | 2.96 | 3.62 | 0.62 |
| VCC 1869 | 1 | 4.30 | 3.42 | 17.0 | 2.35 | 18.38 | 0.69 | 3.60 | 3.64 | 0.63 |
| VCC 1883 | 1 | 2.69 | 1.78 | 17.0 | 2.17 | 16.53 | 0.09 | 2.91 | 4.35 | 0.34 |
| VCC 1903 | 0 | 7.67 | 4.12 | 17.0 | 2.51 | 16.54 | 0.57 | 3.74 | 4.43 | 0.46 |
| VCC 1913 | 0 | 2.69 | 0.63 | 17.0 | 2.10 | 17.00 | 0.20 | 2.90 | 4.09 | 0.31 |
| VCC 1918 | 12 | 1.22 | 0.44 | 17.0 | 1.53 | 22.42 | 0.13 | 2.04 | 1.89 | 0.95 |
| VCC 1923 | 6 | 2.88 | 2.00 | 17.0 | 1.97 | 18.45 | 0.24 | 2.74 | 3.50 | 0.48 |
| VCC 1929 | 8 | 3.09 | 1.35 | 17.0 | 1.99 | 20.43 | 0.48 | 2.94 | 2.77 | 0.82 |
| VCC 1932 | 7 | 3.63 | 1.10 | 17.0 | 2.18 | 17.70 | 0.30 | 3.09 | 3.89 | 0.51 |
| VCC 1938 | 1 | 2.51 | 1.78 | 17.0 | 2.27 | 15.12 | 0.08 | 3.06 | 4.90 | 0.14 |

TABLE 1. (continue)

| Denomination CGGC / VCC | type | a ' | b ' | Dist. Mpc | log V km s ⁻¹ | μ_e mag arcsec ⁻² | log r _e kpc | κ_1 | κ_2 | κ_3 |
|----------------------------|------|--------|--------|--------------|-----------------------------|-------------------------------------|---------------------------|------------|------------|------------|
| VCC 1943 | 5 | 3.98 | 2.51 | 17.0 | 2.25 | 17.51 | 0.30 | 3.18 | 4.01 | 0.55 |
| VCC 1972 | 7 | 3.24 | 2.69 | 17.0 | 2.23 | 18.16 | 0.49 | 3.29 | 3.70 | 0.56 |
| VCC 1978 | 1 | 6.31 | 6.31 | 17.0 | 2.68 | 15.88 | 0.53 | 3.95 | 4.80 | 0.53 |
| VCC 1987 | 7 | 6.17 | 3.24 | 17.0 | 2.24 | 18.38 | 0.67 | 3.43 | 3.57 | 0.52 |
| VCC 1992 | 12 | 0.81 | 0.51 | 17.0 | 1.80 | 23.03 | 0.44 | 2.64 | 1.78 | 1.22 |
| VCC 2000 | 0 | 2.14 | 1.41 | 17.0 | 2.42 | 14.62 | -0.16 | 3.09 | 5.28 | 0.33 |
| VCC 2023 | 7 | 2.51 | 1.26 | 17.0 | 2.00 | 20.43 | 0.47 | 2.95 | 2.78 | 0.83 |
| VCC 2058 | 7 | 7.24 | 5.50 | 17.0 | 2.11 | 19.29 | 0.67 | 3.24 | 3.16 | 0.58 |
| VCC 2092 | 1 | 5.03 | 2.35 | 17.0 | 2.45 | 16.86 | 0.48 | 3.60 | 4.31 | 0.52 |
| VCC 2095 | 1 | 8.70 | 1.95 | 17.0 | 2.32 | 16.20 | 0.55 | 3.46 | 4.39 | 0.17 |
| CGCG 69036 | 5 | 1.20 | 0.89 | 17.0 | 2.26 | 17.61 | -0.01 | 2.97 | 4.11 | 0.76 |
| CGCG 41041 | 8 | 3.80 | 2.40 | 17.0 | 2.11 | 19.69 | 0.56 | 3.18 | 3.08 | 0.74 |
| CGCG 13104 | 1 | 3.80 | 1.10 | 17.0 | 2.37 | 15.45 | 0.13 | 3.24 | 4.85 | 0.31 |
| CGCG 98129 | 0 | 1.60 | 1.08 | 17.0 | 1.95 | 17.16 | -0.01 | 2.54 | 4.00 | 0.29 |
| CGCG 14063 | 7 | 11.00 | 2.05 | 17.0 | 2.17 | 19.21 | 0.93 | 3.51 | 3.13 | 0.49 |
| CGCG 14083 | 0 | 1.90 | 1.10 | 17.0 | 2.30 | 16.84 | 0.00 | 3.04 | 4.39 | 0.62 |
| CGCG 14110 | 7 | 3.20 | 1.37 | 17.0 | 2.12 | 18.73 | 0.45 | 3.10 | 3.44 | 0.59 |
| CGCG 100004 | 7 | 3.90 | 2.76 | 17.0 | 2.40 | 17.09 | 0.30 | 3.40 | 4.28 | 0.63 |
| CGCG 43034 | 7 | 3.60 | 2.99 | 17.0 | 2.17 | 17.89 | 0.11 | 2.93 | 3.90 | 0.65 |
| CGCG 43041 | 7 | 3.20 | 2.16 | 17.0 | 2.01 | 19.00 | 0.40 | 2.92 | 3.29 | 0.56 |
| CGCG 71060 | 9 | 2.20 | 0.61 | 17.0 | 2.24 | 17.82 | 0.16 | 3.08 | 3.96 | 0.69 |
| CGCG 43054 | 8 | 1.50 | 1.09 | 17.0 | 1.73 | 17.64 | -0.12 | 2.15 | 3.72 | 0.22 |

